

The Scales and Equilibration of Midocean Eddies: Forced–Dissipative Flow

K. SHAFER SMITH AND GEOFFREY K. VALLIS

GFDL, Princeton University, Princeton, New Jersey

(Manuscript received 25 January 2001, in final form 16 October 2001)

ABSTRACT

The statistical dynamics of midocean eddies, generated by baroclinic instability of a zonal mean flow, are studied in the context of homogeneous stratified quasigeostrophic turbulence. Existing theory for eddy scales and energies in fully developed turbulence is generalized and applied to a system with surface-intensified stratification and arbitrary zonal shear. The theory gives a scaling for the magnitude of the eddy potential vorticity flux, and its (momentum conserving) vertical structure. The theory is tested numerically by varying the magnitude and mode of the mean shear, the Coriolis gradient, and scale thickness of the stratification and found to be partially successful. It is found that the dynamics of energy in high ($m > 1$) baroclinic modes typically resembles the turbulent diffusion of a passive scalar, regardless of the stratification profile, although energy in the first mode does not. It is also found that surface-intensified stratification affects the baroclinicity of flow: as thermocline thickness is decreased, the (statistically equilibrated) baroclinic energy levels remain nearly constant but the statistically equilibrated level of barotropic eddy energy falls. Eddy statistics are found to be relatively insensitive to the magnitude of linear bottom drag in the small drag limit. The theory for the magnitude and structure of the eddy potential vorticity flux is tested against a 15-layer simulation using profiles of density and shear representative of those found in the mid North Atlantic; the theory shows good skill in representing the vertical structure of the flux, and so might serve as the basis for a parameterization of eddy fluxes in the midocean. Finally, baroclinic kinetic energy is found to concentrate near the deformation scale. To the degree that surface motions represent baroclinic eddy kinetic energy, the present results are consistent with the observed correlation between surface eddy scales and the first radius of deformation.

1. Introduction

Midocean eddies are largely maintained by baroclinic instability, as are their tropospheric counterparts. However, the environment in which such eddies grow and decay is different in the two media. In the atmosphere the scale of the eddies is comparable to the scale of the mean flow itself, and the eddies have a first-order feedback on that mean flow, effecting a significant fraction of the poleward heat transport and substantially reducing the shear of the zonal flow from that of an atmosphere without eddies. By contrast, in the ocean the deformation radius is of order 100 km, at least an order of magnitude smaller than the major ocean basins. Furthermore, and perhaps of greater qualitative import, in the troposphere the profile of static stability (N^2) is roughly constant with height, whereas in the ocean N^2 varies by over an order of magnitude, primarily because of the presence of the main thermocline in the upper 1000 m of the ocean. For these reasons we may expect at least quantitative, and possibly qualitative, differences

in the structure of baroclinic eddies in the ocean and atmosphere.

Approaches to the eddy problem—that is, understanding the mechanisms determining the scales and transport properties of baroclinic eddies—have taken distinct paths, and this in turn has led to different approaches to parameterizing eddies (Green 1970; Stone 1972; Holloway 1986; Vallis 1988; Gent and McWilliams 1990; Visbeck et al. 1997; Killworth 1997; Treguier et al. 1997; and others). The differences arise largely with regard to the assumptions one can make about the degree to which nonlinearity exerts control over the eddies. Killworth (1997), for example, presumes that the eddy flow is weakly nonlinear, specifically that eddy time and space scales can be estimated by local linear stability calculations; this is motivated by the approach of Green (1970) to eddy parameterization in the atmosphere, in which the structure of the eddies is assumed to be that given by linear theory, leaving only the amplitude to be determined by energetic arguments. In contrast, theories such as those of Larichev and Held (1995) assume the steady-state system to be characterized by fully developed geostrophic turbulence, involving significant internal scale transformations between eddy generation and dissipation.

Corresponding author address: K. Shafer Smith, Geophysical Fluid Dynamics Laboratory, P.O. Box 308, Princeton, NJ 08542.
E-mail: kss@gfdl.noaa.gov

pation. In the ocean both the scale separation between the deformation scale and the basin scale, and the dominance of eddy energy over the energy in the mean flow, suggest that it may be fruitful to assume that the evolution of mesoscale eddies is determined by fully nonlinear dynamics, and this is the approach we follow.

This paper is a sequel to Smith and Vallis (2001, hereafter SV), who examined the effects of the background stratification and the Coriolis gradient (β) on the life cycles of baroclinic eddies. One result of SV was that nonuniform stratification makes the transfer between baroclinic modes and the barotropic mode less direct and less efficient [consistent with the earlier analytical work of Fu and Flierl (1980)], leading to the important consequence that significant energy is concentrated in the first baroclinic mode near the radius of deformation. In this paper we examine the forced–dissipated case and include forcing by the baroclinic instability of a zonal mean flow and dissipation by linear bottom drag. The primary questions that we seek to address are

- 1) Given the structure of the mean, baroclinically unstable, zonal flow, what are the scales and structure of the resulting, statistically equilibrated, mesoscale eddies?
- 2) What can one then say about the magnitude and vertical structure of the eddy potential vorticity flux implied by the presence of the eddy field?

Our goal is a “mean field theory,” which describes eddy energy levels and spatial scales as functions of the external parameters in the horizontally homogeneous limit with general, but fixed, mean stratification and zonal shear. We assume that the mean shear and stratification are primarily set by the large-scale wind-driven and thermohaline circulation and that, in steady-state, long-term eddy adjustments are included in that mean. That a mean field theory exists is suggested by the work by Larichev and Held (1995), and Held and Larichev (1996, hereafter HL), who devise a theory for eddy statistics in two (equal) layer, homogeneous quasigeostrophic dynamics. Subsequent numerical tests demonstrated some predictive skill for the bulk eddy quantities. Most notably, their results appear to demonstrate that such quantities follow distinct power law behavior with respect to the mean parameters: given how little is understood of the detailed interactions involved in turbulent flows, the dependencies of eddy quantities on mean flow characteristics might have been hopelessly complicated. Spall (2000) has recently presented some related simulations. Ours differ in that we consider the effects of nonuniform stratification and in the presence of a higher baroclinic modes. However, unlike Spall, we do not examine the effects of nonzonal flow.

The paper is structured as follows. In section 2 we review the quasigeostrophic equations of motion and give their projection onto the vertical modes of the stratification. In section 3 we review the two-mode scaling

theory of Held and Larichev (1996), extending where appropriate to generalize the form of the eddy diffusivity and spectra of baroclinic energy. The ensuing theory is tested in section 4 via a set of numerical simulations in which flows are forced by zonal shears that project onto the first baroclinic mode—here we investigate the sensitivity of such flows to variations in the mean shear, the Coriolis gradient, the scale depth of the stratification, and the bottom drag. The theory is extended to systems with arbitrary shear in section 5. In section 6 we discuss a set of simulations in which the zonal shear projects onto a single higher baroclinic mode and finally consider an integration with relatively high vertical resolution (15 layers) whose modal projection is arbitrary. Some conclusions are provided in section 7. A brief synopsis of the mechanisms of cascade halting is covered in appendix A and some derivations of modal expansions of eddy generation and potential vorticity flux are presented in appendix B.

2. Quasigeostrophy: Modes and layers

The quasigeostrophic equations of motion in the presence of a mean zonal shear are

$$\frac{\partial q'}{\partial t} + J(\psi', q') + \bar{u} \frac{\partial q'}{\partial x} + \frac{\partial \bar{q}}{\partial y} \frac{\partial \psi'}{\partial x} = d, \quad (2.1)$$

where ψ is the streamfunction of the flow, defined such that velocities are $u = -\partial\psi/\partial y$ and $v = \partial\psi/\partial x$, and d represents dissipation terms. The mean potential vorticity gradient is

$$\frac{\partial \bar{q}}{\partial y} = \beta - \frac{d}{dz} \left(\frac{f^2}{N^2} \frac{d\bar{u}}{dz} \right) \quad (2.2)$$

and the perturbation potential vorticity is

$$q'(x, y, z, t) = \nabla^2 \psi' + \frac{\partial}{\partial z} \left(\frac{f^2}{N^2} \frac{\partial \psi'}{\partial z} \right). \quad (2.3)$$

Here $N = N(z)$ is the local buoyancy frequency, f is the local Coriolis frequency, and β is its local meridional gradient. Our notation convention is that an overbar (\bar{A}) implies a *horizontal* spatial average, a prime (A') denotes a deviation from this average, and angle brackets ($\langle A \rangle = \overline{A'^2}$) denote a root-mean-square (rms) value. A tilde (\tilde{A}) will also be used to a representative magnitude for scaling purposes.

One can project quasigeostrophic motion onto the neutral stratification modes, which are solutions of the eigenvalue problem (see, e.g., Hua and Haidvogel 1986)

$$\frac{\partial}{\partial z} \left(\frac{f^2}{N^2(z)} \frac{\partial \phi}{\partial z} \right) = -\lambda^2 \phi, \quad z \in (-H, 0), \quad (2.4)$$

with the boundary conditions $\phi_z(z = 0, -H) = 0$ (i.e., a rigid lid and flat bottom). The eigenvalues λ are thus

the baroclinic deformation wavenumbers. The modes are orthogonal, and may be normalized so that

$$\frac{1}{H} \int_{-H}^0 \phi_m \phi_n dz = \delta_{mn}, \quad (2.5)$$

where the subscripts denote the mode numbers ($m = 0$ for the barotropic mode, $m = 1$ for the first baroclinic mode, etc.). Since the modes are complete, one may represent the vertical structure of the potential vorticity by an expansion in these modes

$$q(x, y, z, t) = \sum_{m=0}^{\infty} Q_m(x, y, t) \phi_m(z), \quad (2.6)$$

and similarly for the streamfunction

$$\psi(x, y, z, t) = \sum_{m=0}^{\infty} \Psi_m(x, y, t) \phi_m(z). \quad (2.7)$$

For space-dependent variables, lowercase symbols will denote z -coordinate fields, while uppercase symbols denote the modal projection of a field—thus, Ψ_m is the modal projection of ψ . Upon substitution into the quasi-geostrophic equation of motion and integration over z , one arrives at the modal equation of motion for the fully stratified case

$$\frac{\partial Q'_m}{\partial t} + \sum_{ij} \xi_{ijm} J(\Psi'_i, Q'_j) + \beta \frac{\partial \Psi'_m}{\partial x} = F_m + D_m, \quad m = 0, N - 1, \quad (2.8)$$

where D_m represent dissipation terms and

$$F_m = \sum_{ij} \bar{U}_j \xi_{ijm} \frac{\partial}{\partial x} (Q'_i + \lambda_j^2 \Psi'_i) \quad (2.9)$$

is the forcing. The modal potential vorticity is

$$Q'_m(x, y, t) = (\nabla^2 - \lambda_m^2) \Psi'_m(x, y, t) = \frac{1}{H} \int_{-H}^0 \phi_m(z) q(x, y, z, t) dz, \quad (2.10)$$

and modal horizontal velocities are

$$U'_m(x, y, t) = -\frac{\partial \Psi'_m}{\partial y}(x, y, t) = \frac{1}{H} \int_{-H}^0 \phi_m(z) u(x, y, z, t) dz, \quad (2.11)$$

$$V'_m(x, y, t) = \frac{\partial \Psi'_m}{\partial x}(x, y, t) = \frac{1}{H} \int_{-H}^0 \phi_m(z) v(x, y, z, t) dz. \quad (2.12)$$

The triple interaction coefficient is

$$\xi_{ijm} = \frac{1}{H} \int_{-H}^0 \phi_i \phi_j \phi_m dz. \quad (2.13)$$

Note that $\xi_{ij0} = \delta_{ij}$ and that ξ_{ijm} is symmetric with respect to permutations of its indices. Further selection rules for the interaction coefficient exist only in the case of a linear density profile (i.e., constant N^2).

3. Steady-state statistics in the two-mode case

The simplest baroclinic system is the two-layer model. This may be thought of as a crude representation of a realizable physical system, or as representing the two gravest vertical modes of the fully stratified system. Energy injected into higher vertical modes will cascade toward the graver modes, with no significant cascade toward higher vertical modes (Charney 1971). Thus if the mean shear of a stratified flow projects primarily onto the first baroclinic mode, thereby generating predominantly first-mode baroclinic eddy energy, the higher vertical modes should play at most a catalytic role in the transfer of energy between the first baroclinic and barotropic modes—just as there is no significant energy flux toward horizontal scales smaller than the energy injection scale in two-dimensional turbulence, there is none toward smaller vertical scales in geostrophic turbulence. However, in two-dimensional turbulence the enstrophy cascade must be somewhat resolved in order to properly simulate the inverse cascade of energy, and similarly some higher vertical modes must be represented in order to properly represent the cascade toward the barotropic mode in geostrophic turbulence. Barnier et al. (1991), for example, found a similar result in six-layer simulations of a wind-driven gyre.

Let us consider the case in which only first-mode baroclinic energy is generated and ignore the contributions of higher modes. As in standard turbulence phenomenology we will assume that inertial ranges, with constant fluxes of energy, exist. The two-mode equations can be obtained by presuming no amplitude in modes $m > 1$, in which case (2.8) becomes

$$\frac{\partial \nabla^2 \Psi'_0}{\partial t} + J[\Psi'_0, \nabla^2 \Psi'_0] + J[\Psi'_1, \nabla^2 \Psi'_1] + \beta \frac{\partial \Psi'_0}{\partial x} = \bar{U} \frac{\partial \nabla^2 \Psi'_1}{\partial x} + D_0, \quad (3.1a)$$

$$\frac{\partial (\nabla^2 - \lambda^2) \Psi'_1}{\partial t} + J[\Psi'_0, (\nabla^2 - \lambda^2) \Psi'_1] + J[\Psi'_1, \nabla^2 (\Psi'_0 + \xi \Psi'_1)] + \beta \frac{\partial \Psi'_1}{\partial x} = \bar{U} \frac{\partial}{\partial x} [\nabla^2 (\Psi'_0 + \xi \Psi'_1) + \lambda^2 \Psi'_0] + D_1, \quad (3.1b)$$

where D_0 and D_1 represent dissipation terms. While discussing the two-mode picture we shall write $\lambda = \lambda_1$, $\bar{U} = \bar{U}_1$, and $\xi = \xi_{111}$. Note that if $\xi = \beta = 0$, we recover Eqs. (4a,b) of Larichev and Held (1995).

Rhines (1977) and Salmon (1980) proposed (3.1) as a model of the baroclinic eddy cycle. In this picture, baroclinic eddy energy is generated by a baroclinically unstable mean state, and ultimately transferred via nonlinear interactions to large horizontal scale in the barotropic mode, where it is then dissipated by Ekman drag in the boundary layer. The transfer occurs as follows: in the limit of scales large compared to the radius of deformation, or wavenumber $K \ll \lambda$, and equal layer thicknesses, the baroclinic equation of motion (3.1b) can be approximated as the advection of a passive tracer by the barotropic flow, or

$$\frac{\partial \Psi_1}{\partial t} + J(\Psi_0, \Psi_1 - \bar{U}y) = -\lambda^{-2}D_1, \quad (3.2)$$

and the barotropic equation (3.1a) can be approximated as two-dimensional turbulence stirred by transfers from the baroclinic field [consider terms involving Ψ_1 in (3.1a) to be right-hand side forcing terms]. The variance of Ψ_1 , that is, baroclinic eddy available potential energy, is generated at large horizontal scale by an imposed large-scale mean gradient, $-\bar{U}y$, and cascades downscale toward the radius of deformation. These nonlinear baroclinic transfers stir the barotropic mode, effecting a conversion of baroclinic energy to barotropic kinetic energy, which then cascades upscale until halted by some competing process. Specifically, Rhines proposed that the barotropic cascade is halted by the β effect. In steady state then, the baroclinic and barotropic dynamics are intertwined, with deformation scale transfers from the baroclinic mode stirring the barotropic mode, and the ensuing large-scale concentration of barotropic energy engendering large-scale eddy generation in the baroclinic mode.

Held and Larichev built upon the above picture to form a closed set of algebraic scaling equations for the rms barotropic eddy velocity $\langle V'_0 \rangle$, the total eddy generation rate g , and the horizontal scale of barotropic eddies K_0^{-1} in terms of the external parameters \bar{U} , β , and λ . We argue that this theory applies to the fully stratified case when the mean shear is predominantly first-baroclinic, with some caveats. In order to build upon HL, we summarize their arguments.

It is assumed that 1) baroclinic transfers are localized near the deformation scale, 2) generation is localized near the energy containing scales, 3) dissipation occurs predominantly at large scale, 4) horizontal energy transfers are spectrally local, and 5) that $K_0 \ll \lambda$ in steady state. Then at scales large compared to λ^{-1} , one expects a constant *inverse* barotropic spectral flux ϵ_0 and a barotropic energy density spectrum

$$E_0(K) = C_0 \epsilon_0^{2/3} K^{-5/3}, \quad (3.3)$$

where C_0 is the Kolmogorov constant for the barotropic flow. One also expects baroclinic available potential energy (which is approximately total energy at $K \ll \lambda$) to have the spectrum of a passive tracer advected by the barotropic flow, or

$$E_1(K) = C_1 \epsilon_1 \epsilon_0^{-1/3} K^{-5/3}, \quad (3.4)$$

where C_1 is the baroclinic Kolmogorov constant and ϵ_1 is the baroclinic flux (Larichev and Held 1995). It is further argued that the cascade is halted at the Rhines scale,

$$K_0 \approx \beta^{1/2} \langle V'_0 \rangle^{-1/2}, \quad (3.5)$$

at which point nonlinear transfers can no longer proceed efficiently.

The localizations of generation and transfer imply that the upscale barotropic and downscale baroclinic spectral fluxes, if constant in the inertial range, are also equal to one another, and further equal to the eddy generation rate g , hence

$$\epsilon_0 = \epsilon_1 = g. \quad (3.6)$$

In the two vertical mode quasigeostrophic system the eddy generation due to baroclinic instability [the only nonvanishing source term in the energy equation derived from the baroclinic equation of motion (3.1b)] is

$$g = \bar{U} \lambda^2 \overline{V'_0 \Psi'_1} \quad (3.7)$$

for which a scaling estimate is needed. Assume a priori that $\langle V'_0 \rangle \gg \langle V'_1 \rangle$ (since one expects energy to collect at large scale in the gravest mode) and that the spectra for the barotropic velocity is strongly peaked at wavenumber K_0 . Thus $\overline{V'_0 \Psi'_1} \approx \langle V'_0 \rangle \langle \Psi'_1 \rangle_{K_0}$, where $\langle \rangle_{K_0}$ means the rms value in the *neighborhood* of K_0 in the spectral sense. Further assume $\langle \Psi'_1 \rangle_{K_0} \approx K_0^{-1} \langle V'_1 \rangle_{K_0}$ so that

$$g \approx \bar{U} \lambda^2 K_0^{-1} \tilde{V}_0 \hat{V}_1, \quad (3.8)$$

where we have defined $\tilde{V}_0 \equiv \langle V'_0 \rangle$ and $\hat{V}_1 \equiv \langle V'_1 \rangle_{K_0}$ —only baroclinic velocities near the mixing length are important in the correlation, which determines the generation (3.7). Note that the presumption that eddy generation occurs at large horizontal scale (Larichev and Held 1995) is implicit in the scaling of the correlation term in (3.8).

One can relate the barotropic flux, and hence the generation rate, to the rms velocity by integrating the barotropic energy density (3.3). Specifically,

$$\frac{\langle V'_0 \rangle^2}{2} \approx \int_{K_0}^{\lambda \gg K_0} C_0 \epsilon_0^{2/3} K^{-5/3} dK \Rightarrow \epsilon \approx \alpha^{-1} \tilde{V}_0^3 K_0, \quad (3.9)$$

where $\alpha \equiv (3C_0)^{3/2}$. Substitution of (3.9) and (3.8) into (3.6) yields

$$\tilde{V}_0 \approx (\alpha \bar{U} \hat{V}_1)^{1/2} \lambda K_0^{-1}. \quad (3.10)$$

Substitution of the Rhines scale (3.5) into (3.8) and (3.10) then gives

$$\tilde{V}_0 \approx (\alpha \bar{U} \hat{V}_1) \lambda^2 \beta^{-1}, \quad (3.11a)$$

$$K_0 \approx (\alpha \bar{U} \hat{V}_1)^{-1/2} \lambda^{-1} \beta, \quad (3.11b)$$

$$g \approx \alpha^{-1} (\alpha \bar{U} \hat{V}_1)^{5/2} \lambda^5 \beta^{-1}. \quad (3.11c)$$

The system is not closed since no estimate for the baroclinic eddy velocity \hat{V}_1 has been suggested. Two arguments for this quantity are presented below.

a. Diffusion of potential vorticity

Assuming eddy potential vorticity is diffused down its mean gradient, one can write

$$\overline{v'q'} \approx -D \frac{\partial \bar{q}}{\partial y}, \quad (3.12)$$

where D is the diffusivity. This is equivalent to assuming that rms baroclinic eddy velocities near the energy containing scale (K_0^{-1}) take on the value of the mean baroclinic flow, thus $\langle V'_1 \rangle_{K_0} \approx \bar{U}$. To see this, evaluate the left-hand side (lhs) and right-hand side (rhs) of (3.12) separately and compare terms.

Expanding the lhs in terms of modes and estimating the correlation term, one finds

$$\begin{aligned} \overline{v'q'} &\approx \overline{V'_0 Q'_1} \approx \lambda^2 \langle V'_0 \rangle \langle \Psi'_1 \rangle_{K_0} \\ &\sim \lambda^2 K_0^{-1} \langle V'_0 \rangle \langle V'_1 \rangle_{K_0}, \end{aligned} \quad (3.13)$$

where the modal expansion and estimate of the potential vorticity flux discussed in appendix B is used in the first line, an estimate of potential vorticity ($\langle Q_1 \rangle \approx \lambda^2 \langle \Psi_1 \rangle$) at scales $K \ll \lambda$ is used in the second line, and the estimate $\Psi'_1 \sim V'_1 K_0^{-1}$ is used in the third line.

The rhs can be estimated from the mean potential vorticity gradient $\partial \bar{q} / \partial y = \beta - \lambda^2 \bar{U}$ in the strongly unstable limit ($\beta \ll \bar{U} \lambda^2$), and assuming a diffusivity given by the length and velocity scales of the energy containing eddies, $D \approx \langle V'_0 \rangle K_0^{-1}$. The rhs is then

$$-D \frac{\partial \bar{q}}{\partial y} \sim \langle V'_0 \rangle K_0^{-1} \bar{U} \lambda^2. \quad (3.14)$$

Comparing (3.13) and (3.14), one finds

$$\langle V'_1 \rangle_{K_0} \sim \bar{U}. \quad (3.15)$$

The results of HL are recovered when (3.15) is substituted into the scaling relations (3.11) (apart from the nondimensional constants which we have included). In this case the effective eddy diffusivity is $D \sim \bar{U}^3 \lambda^3 / \beta^2$, where D is defined in (3.12).

b. Including another length scale

One can alternatively estimate \hat{V}_1 as follows. The present derivation is similar to the derivation of the relation between the rms barotropic velocity variance and the spectral flux (3.9). At scales much larger than the deformation scale, the total baroclinic energy density $E_1 \approx \lambda^2 |\Psi_1|^2 = A_1$, where A_1 is the available potential

energy. The baroclinic kinetic energy is then $T_1 = K^2 |\Psi_1|^2 \approx (K^2 / \lambda^2) E_1$ for $K \ll \lambda$, or specifically, using the passive scalar spectrum (3.4),

$$T_1(K) \approx C_1 \lambda^{-2} \epsilon^{2/3} K^{1/3}, \quad (3.16)$$

where $\epsilon \equiv \epsilon_0 = \epsilon_1$. On scales $K \gg \lambda$, one reverts to either a K^{-3} spectrum, now because small-scale baroclinic enstrophy behaves as in two-dimensional turbulence and cascades downscale, or, if there is some stirring at much smaller scales, a $K^{-5/3}$ spectrum up to the deformation scale. In either case, these arguments imply a peak in baroclinic kinetic energy near $K \sim \lambda$. This is a generalization to the forced-dissipative case of the result found in SV, and is roughly consistent with observations (Stammer 1997) that show a correlation of surface eddy scales to the local first radius of deformation.

By definition,

$$\begin{aligned} \frac{\hat{V}_1^2}{2} &= \frac{\langle V'_0 \rangle_{K_0}^2}{2} \\ &= \int_{K_0}^{K_0 + \Delta} T_1(K) dK \xrightarrow{\Delta \ll K_0} T_1(K_0) \Delta, \end{aligned} \quad (3.17)$$

where Δ is the range of wavenumbers over which baroclinic energy is significant. Using (3.16) and the scaling relations (3.11) one finds

$$\hat{V}_1 \approx (2C_1)^2 \alpha^{5/3} (\lambda \Delta \beta^{-1})^2 \bar{U}^3. \quad (3.18)$$

Larichev and Held (1995) argue that, when no other length scale exists, $\Delta \approx K_0$, in which case, using the expression for K_0 in (3.11), one is left with turbulent diffusion,

$$\hat{V}_1 \approx (2C_1 \alpha^{1/3}) \bar{U}. \quad (3.19)$$

Using (3.19) in (3.11) gives us

$$\tilde{V}_0 \approx \gamma T_e^{-2} \beta^{-1}, \quad (3.20a)$$

$$K_0 \approx \gamma^{-1/2} T_e \beta, \quad (3.20b)$$

$$g \approx \alpha^{-1} \gamma^{5/2} T_e^{-5} \beta^{-1}, \quad (3.20c)$$

$$\hat{V}_1 / \bar{U} \approx \alpha^{-1} \gamma = \text{const}, \quad (3.20d)$$

where

$$T_e^{-1} = \bar{U} \lambda \quad (3.21)$$

is the eddy timescale and $\gamma = 2C_1 \alpha^{4/3}$. Equations (3.20) are the predictions of HL (apart from the nondimensional constants). Assuming, on the other hand, that the spectral width Δ of the barotropic velocity variance is independent of the scale K_0 itself, and substituting (3.18) into the scalings (3.11) yields

$$\tilde{V}_0 \approx (\gamma \Delta)^2 T_e^{-4} \beta^{-3}, \quad (3.22a)$$

$$K_0 \approx (\gamma \Delta)^{-1} T_e^3 \beta^2, \quad (3.22b)$$

$$g \approx \alpha^{-1} (\gamma \Delta)^5 T_e^{-10} \beta^{-7}, \quad (3.22c)$$

$$\hat{V}_1 / \bar{U} \approx \alpha^{-1} (\gamma \Delta)^2 T_e^{-2} \beta^{-2}. \quad (3.22d)$$

In either case (and as pointed out for the former by HL) the eddy timescale is a function only of the mean flow—changes in the strength and diffusivity of the eddy flow are due to the change in length scale, which results from the inverse cascade. Note that we have retained non-dimensional constants due to their expected nonnegligible magnitudes—using $C_0 = 5.58$ (Maltrud and Vallis 1991) and $C_1 = 0.29$ (Lesieur and Herring 1985), one finds that $\alpha = 68.5$ and $\gamma = 163$. Ultimately, however, we will regard the product $\gamma\Delta$ and γ itself as adjustable parameters. The parameter Δ should be regarded as an undetermined addition to the turbulent diffusion theory.

4. Simulations of stratified flow with first baroclinic mode forcing

As claimed earlier, the two-mode simplification is relevant when the mean zonal shear in the fully stratified case projects primarily onto the first baroclinic mode. In this case, so long as the streamfunctions describing the higher modes remain relatively weak (which is expected since they are only forced by any residual up -mode cascade), eddy energy generation will involve only the first baroclinic mode.

In order to test the scalings (3.22) and (3.20), we use a stratified, horizontally spectral quasigeostrophic homogeneous turbulence model, forced by baroclinic instability of a mean zonal shear, and with profiles of stratification and shear that are in general nonconstant with depth. The enstrophy cascade is absorbed by a ∇^8 hyperviscosity and energy is dissipated by a linear drag in the bottom layer, thus referring to (2.1), the dissipation function used is

$$d = -\delta(z + H)r\nabla^2\psi - \nu\nabla^8q, \quad (4.1)$$

where in all cases ν is set adaptively (using the rms vorticity and truncation wavenumber to give time and length scales, respectively—numerical details may be found in SV). The horizontal model dimensions are $2\pi \times 2\pi$ so that wavenumber 1 fills the domain. Time is scaled as \hat{L}/U , where $\hat{L} = L/(2\pi)$, L is the physical domain size and U is a typical flow velocity. Thus the Coriolis gradient $\beta = \beta_*\hat{L}^2/U$ and deformation wavenumbers $\lambda = \lambda_*/L$ (star-subscripted quantities are dimensional).

The following integrations used five layers and 256² equivalent horizontal grid points (truncation wavenumber $K_{\max} = 127$). The first baroclinic deformation wavenumber is held constant at $\lambda_1 = 35$, which allows a significant inverse cascade, giving us room to vary the stopping scale, K_0^{-1} , over a range of values.¹ While the

higher baroclinic deformation wavenumbers vary depending upon the stratification, in the present simulations even the smallest deformation scale is resolved (the scales for the two stratification types are given below). Each run is forced with a mean zonal shear that projects exactly onto the first baroclinic mode with modal coefficient $\bar{U} = \bar{U}_1$. For both uniform and surface intensified stratification, the parameters \bar{U} and β are varied over a range of values. We also discuss sequences of lower resolution simulations in which the stratification scale depth and the bottom drag are systematically varied.

In all simulations described in this paper, the mean flow parameters are chosen such that the stopping scale ranges from a value just smaller than the domain size to just larger than the first deformation scale; in other words, such that the flow varies from weakly to strongly unstable. A measure of the instability of the mean flow is the supercriticality, which, if a single mode m is forced, is written $\bar{U}_m\lambda_m^2\beta^{-1}$ —the supercriticality for all runs discussed varies from about 2 to about 10.

Simulations with nonuniform stratification use an exponential profile for potential density

$$\rho(z)/\rho_0 = 1 + \Delta\rho(1 - e^{\bar{z}/\delta}), \quad (4.2)$$

where $\Delta\rho \equiv (\rho_{\text{bottom}} - \rho_{\text{top}})/\rho_0$ is the fractional change in density over the depth of the ocean, δ is the fractional scale depth, and \bar{z} is the fractional depth coordinate, defined as $\bar{z} \equiv z/H$. In this section, all runs with nonuniform stratification use $\delta = 0.15$, which corresponds to an idealized thermocline-like stratification intended to be representative of the midlatitude oceans. For uniform stratification, the deformation wavenumbers are $\lambda_1 = 35.0$, $\lambda_2 = 65.0$, $\lambda_3 = 89.5$, $\lambda_4 = 105$, and in the nonuniform case they are $\lambda_1 = 35.0$, $\lambda_2 = 71.5$, $\lambda_3 = 102$, $\lambda_4 = 108$. All runs presented in the first two subsections used a bottom drag coefficient of $r = 0.2$, which is small compared to $\bar{U}_1\lambda_1$ for typical values used in these runs ($\lambda_1 = 35$ and $\bar{U} \approx 0.1$). The shear and density profiles used for the present simulations are shown in Fig. 1.

a. Sensitivity to mean shear magnitude

The results from the first set of simulations, in which the imposed mean shear \bar{U} is varied systematically, are presented in Fig. 2. In each of the four panels is a different statistic for the same set of runs, while each data point in a given panel represents the value of that statistic averaged in time and horizontal space during the steady-state phase for a given run. Circles represent runs with uniform stratification and asterisks represent those with exponential stratification ($\delta = 0.15$). All of these runs were performed with fixed $\beta = 50$, and the values of shear used ranged $\bar{U} \in (0.08, 0.21)$. A measure of the instability of the flow is the supercriticality $\bar{U}\lambda_1^2\beta^{-1}$, which ranged from 2.0 to 5.1. The total rms barotropic eddy velocity \tilde{V}_0 (averaged horizontally and

¹ Note that the radius of deformation is set primarily by fixed physical parameters (H_0 , g , ρ_0 , f_0 , $\Delta\rho$), but also by the structure of the density profile (see SV). In the spectral model, the deformation wavenumber is scaled by the size of the domain such that modes with wavenumber 1 fit exactly in the domain. Hence in order to keep λ_1 the same when different vertical density profiles are used, we in essence change the domain scale appropriately. In this way, a constant spectral range is maintained.

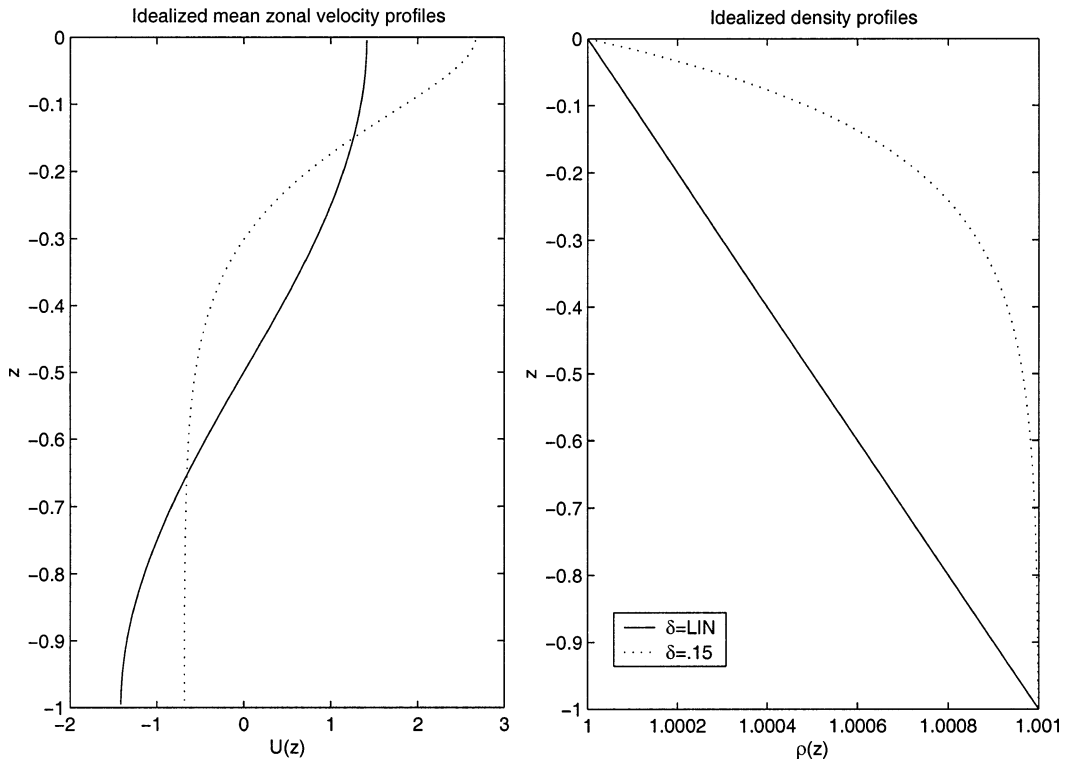


FIG. 1. Profiles of mean zonal velocity (left panel) and mean density (right panel) for simulations in which first baroclinic mode is forced. The two zonal velocity profiles represent the respective shapes of the first baroclinic modes for the density profiles shown.

over many eddy turnaround times) is shown in the upper left panel, and the total rms first baroclinic eddy velocity \tilde{V}_1 is displayed in the upper right panel. A full spatial and time average of the eddy generation (3.7) is shown in the lower left panel of Fig. 2 and the barotropic energy containing wavenumber K_0 (calculated as a centroid over a window of wavenumbers containing the peak) is shown in the bottom right.

The solid lines in Fig. 2 represent the scaling predictions based on the constant Δ theory (3.22) with $\gamma\Delta = 32.1$. This value was chosen as the best fit of theory (constrained to have the slope predicted by the scaling) to the rms barotropic eddy velocity (upper left panel of Fig. 2) for the *uniform* stratification cases (circles). The same value of $\gamma\Delta$ is used for the other three statistics as well (displayed in the other three panels in Fig. 2). The dotted line is the turbulent diffusion prediction of (3.20), with $\gamma = 5.7$. Again, this is the best fit of said theory to the rms barotropic velocity in the case of uniform stratification. Now formally the γ in each case are functions of the same nondimensional Kolmogorov constants [see text following Eq. (3.22)], and γ should have a value near 163, but in both theories the γ factor arises from the considerable assumptions that motivated the integral in (3.17) used to determine the baroclinic rms eddy velocity in the neighborhood of the barotropic mixing scale. So, in some sense, these values are scaling factors for \tilde{V}_1 for which we have given an estimate, but

which we ultimately choose to fit the simulation results. Regardless of their values, we have also propagated the γ factors through the scaling relations (3.11) (in which \tilde{V}_1 was not yet specified), and if the fit to one statistic yields a value that fits the other statistics with some accuracy as well, we can assume at least that the scaling of \tilde{V}_1 was crucial to the underlying theory (for either turbulent diffusion or the constant Δ theory).

The dashed line represents the constant Δ theory modified for nonuniform stratification and, hence, if the modification is valid, should fit the asterisks. Again, the same value of $(\gamma\Delta)$ is used for the dashed lines in each panel. How the dashed line is derived and calculated will be explained in subsection c.

The theories developed in the previous section hinged upon predictions of the rms baroclinic eddy velocity in the neighborhood of K_0 . We do not plot this quantity, however, because consistent determination thereof is ambiguous (we do not know Δ). Instead, in the upper right hand panel of Fig. 2 we plot the *total* baroclinic variance, $\tilde{V}_1 = \langle V_1' \rangle$, which we obtain in the same way as \tilde{V}_0 . Predictions for \tilde{V}_1 are obtained by integrating the theoretical baroclinic kinetic energy (3.16) over the relevant part of the spectrum and using the respective scaling estimates for the turbulent diffusion (3.20) and constant Δ (3.22) scaling theories to close the equation and solve for \tilde{V}_1 . In particular, the baroclinic kinetic energy spectrum (3.16) is valid for the inertial energy range

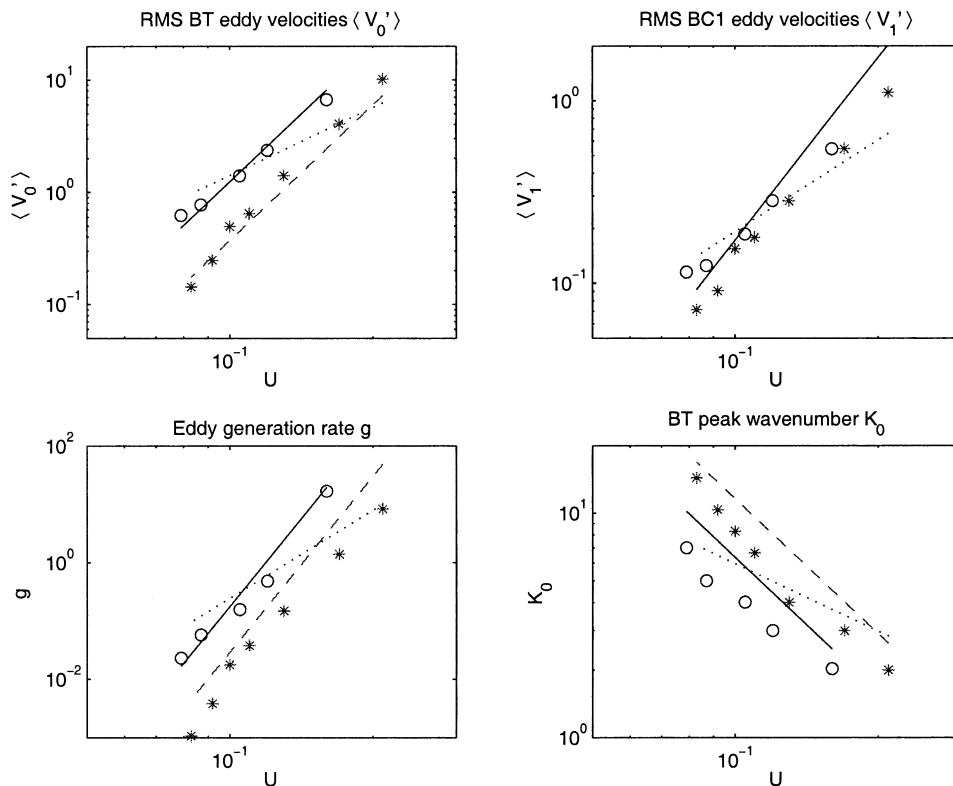


FIG. 2. Statistics from sequence of 5 layer by 256^2 simulations in which the amplitude of the mean shear, which projects exactly onto the first baroclinic mode, is varied. The figures are as follows. (Top left) rms barotropic eddy velocity \tilde{V}_0 ; (top right) rms first baroclinic eddy velocity \tilde{V}_1 ; bottom left panel: rms eddy generation rate g ; bottom right panel: barotropic kinetic energy centroid K_0 . The values of shear range from $\bar{U} = 0.08$ to 0.21 . Fixed parameters are $\beta = 50$, $\lambda_1 = 35$ and $r = 0.2$. A measure of the instability of the flow is the supercriticality $\bar{U}\lambda_1^2\beta^{-1}$, which ranges from 2.0 to 5.1 for these simulations. Each circle represents a value from an equilibrated run with uniform stratification and each asterisk a value from a run with an exponential density profile of scale depth $\delta = 0.15$. The dotted lines represent the scalings predicted by classic turbulent diffusion (3.20) and the solid lines represent the predictions modified by the constant Δ theory (3.22). The dashed line shows the latter theory modified for the effects of the stratification, as per (4.6) and (4.8). Theory for total baroclinic velocity variance is given by (4.4) and (4.5). Since the baroclinic velocity variance does not, and is not expected to vary with stratification scale depth, there is no dashed line in the upper right panel.

and should hold at most up to the deformation scale— at higher wavenumbers the spectrum drops off sharply, and one can make the estimate

$$\frac{\tilde{V}_1}{2} \approx \int_0^{\lambda_1} T_1(K) dK = \frac{3}{4} C_1 \epsilon_1^{2/3} \lambda_1^{-2/3}. \quad (4.3)$$

Using $\epsilon_1 = g$ from the constant Δ scaling (3.22) yields

$$\tilde{V}_1 \approx \left(\frac{3C_1}{2} \right)^{1/2} \alpha^{-1/3} (\gamma\Delta)^{5/3} \lambda^3 \bar{U}^{10/3} \beta^{-7/3}, \quad (4.4)$$

and similarly from turbulent diffusion (3.20) one finds

$$\tilde{V}_1 \approx \left(\frac{3C_1}{2} \right)^{1/2} \alpha^{-1/3} \gamma^{5/6} \lambda^{4/3} \bar{U}^{5/3} \beta^{-2/3}. \quad (4.5)$$

In plotting the above estimates we used $C_1 = 0.3$ and $\alpha = 68.5$.

The results for \tilde{V}_1 do not clearly select between the

proposed theories, yet when folded into the predictions for the barotropic velocity \tilde{V}_0 , the generation rate g , and the stopping scale K_0 , we find that the simulations, at least in this first set of runs, support the constant Δ predictions (3.22). While the offset in the prediction was chosen as the best fit, \tilde{V}_0 varies very nearly like \bar{U}^4 in slope. Furthermore, the slopes of g and K_0 fall near those predicted by (3.22) as well. In magnitude, the propagation of the fits for $\gamma\Delta$ for (3.22) and γ for (3.20) have placed the theoretical fits for \tilde{V}_1 and g very close to the results for both theories. The predictions for K_0 are less accurate, but there is also more margin for error in the determination thereof from the simulation results. In all, the results support the importance of proper scaling of \tilde{V}_1 .

We also show a set of spectra for two of the simulations, one with uniform and the other with surface-intensified stratification, in Fig. 3. Notably, the quali-

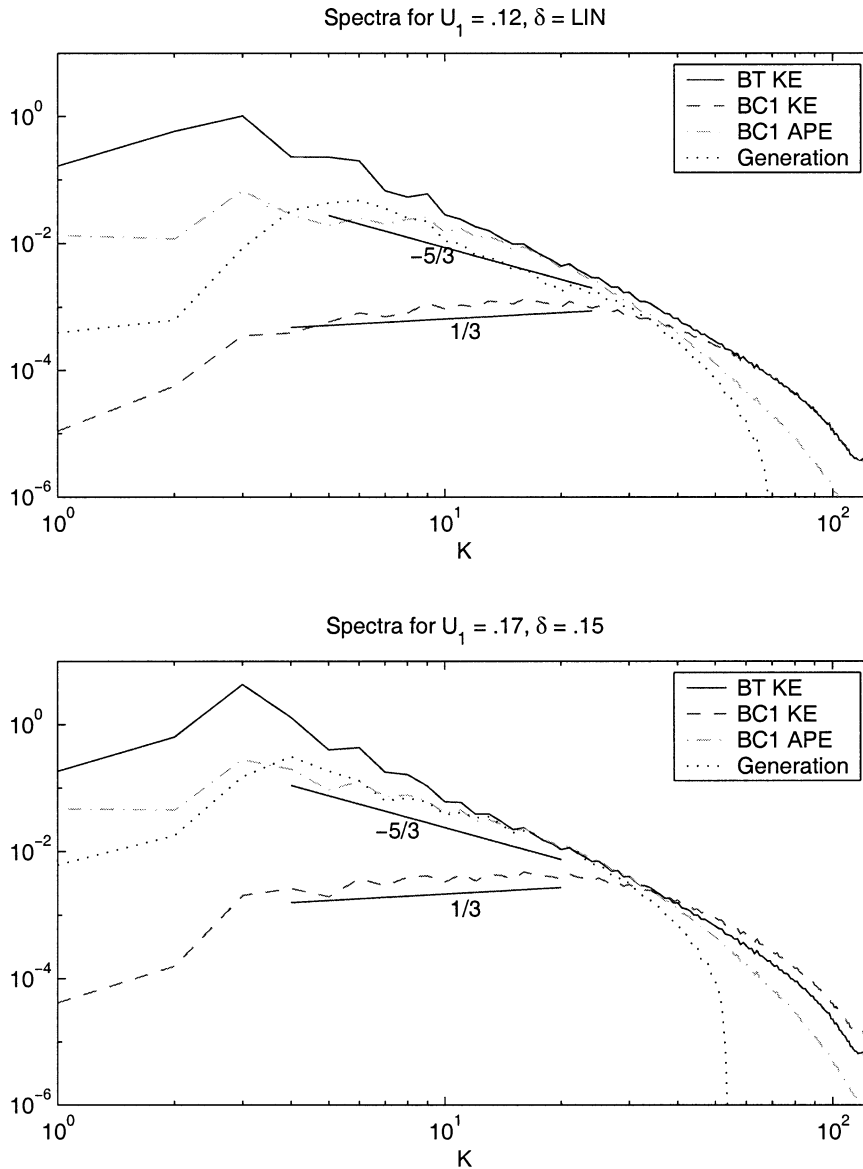


FIG. 3. Spectra of barotropic kinetic energy (solid), first baroclinic kinetic energy (dashed), first baroclinic available potential energy (dash-dotted) and eddy generation rate (dotted): (top) spectra from a uniform stratification run in which the first baroclinic mode is forced ($\bar{U}_1 = 0.12$) and (bottom) the same set of spectra for a similar run, but with surface intensified stratification ($\delta = 0.15$) and $\bar{U}_1 = 0.17$. Also shown are expected slopes for barotropic kinetic and available potential energy ($K^{-5/3}$), and for baroclinic kinetic energy ($K^{1/3}$). The energies of modes not displayed are all at least one order of magnitude smaller than those shown.

tative structure of the two sets of spectra are more alike than not. In both cases we find that the available potential energy (in the first baroclinic mode) and generation rate have spectra close to $K^{-5/3}$, while the barotropic kinetic energy is much steeper with a slope close to K^{-3} . Of these, only the potential energy spectral slope is as expected; in our scaling we assumed implicitly that the generation rate was localized at the mixing scale and that the barotropic kinetic energy possessed a $K^{-5/3}$ slope. These two variations from our expectations are

most probably related: the spectral width of the generation implies a nonconstant inertial range flux (probably accompanied by a spectrally wide transfer between baroclinic and barotropic modes), which is sufficient to alter the slope of the up-scale cascade in the barotropic mode. The first baroclinic kinetic energies in both cases, on the other hand, have slopes close to $K^{1/3}$, as predicted. One should also note that in both cases the baroclinic kinetic energy spectra have peaks near the first baroclinic deformation scale. The energies of modes not

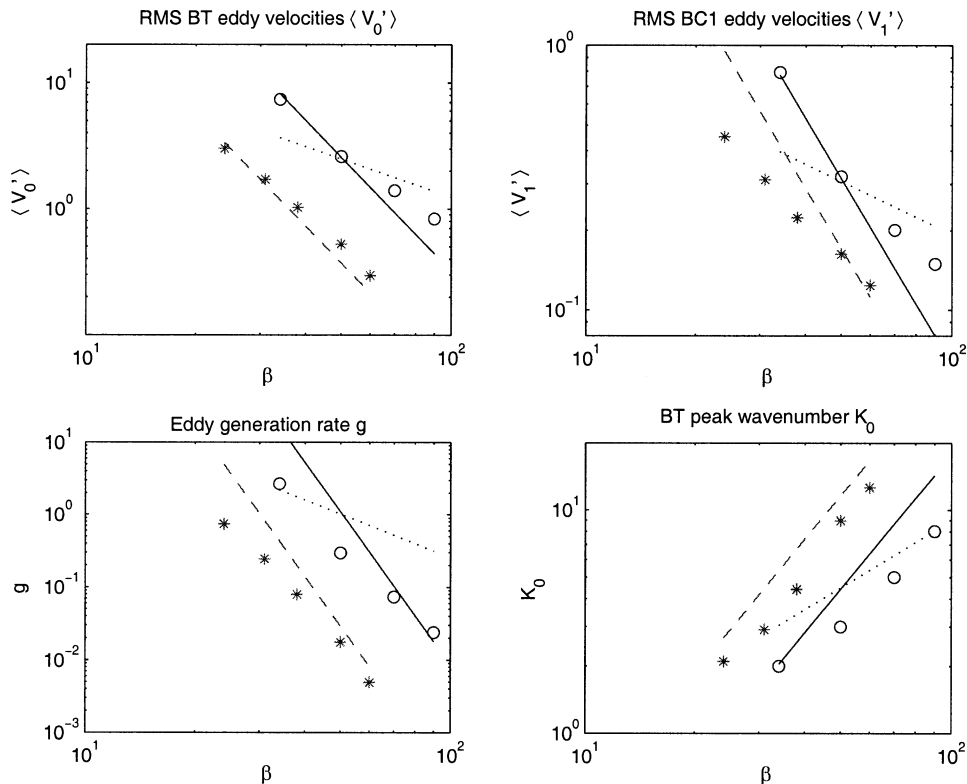


FIG. 4. Statistics from sequence of 5 layer by 256^2 simulations in which β is varied between 22 and 90. The mean zonal shear projects only onto the first baroclinic mode with the value $\bar{U} = 0.12$ for the uniform stratification simulations and $\bar{U} = 0.1$ for the nonuniform stratification simulations. Other parameters are the same as those in sequence of runs in which \bar{U} was varied. Supercriticalities $\bar{U}\lambda_1^2\beta^{-1}$ range from 1.4 to 6.7. Layout is just as for Fig. 2. The presence of the dashed line in the upper right panel is due to the fact that \bar{U} was different for the two sets of simulations (not due to a variation of the baroclinic velocity with stratification).

displayed in the figure are all orders of magnitude smaller than those shown.

As for differences between the two cases due to stratification effects, one finds cleaner inertial range slopes in the *surface-intensified* case, and a sharper peak of barotropic energy at the mixing scale. Differences in overall energy levels will be discussed in the next section (but note that magnitude of the mean shear for the two cases presented is not the same, so differences in energy levels between these two plots cannot be interpreted as due to differences in stratification depth δ).

b. Sensitivity to β

In Fig. 4 we show the results from a set of simulations similar to those discussed in the previous subsection, except in this case β is varied while the mean zonal shear is held constant at $\bar{U} = 0.12$ for the uniform stratification case and $\bar{U} = 0.1$ for the surface-intensified case. These are central values from the ranges used in the constant β simulations (accidentally, there was no common central value of \bar{U} in those runs, but this does not affect any of our arguments). The Coriolis gradient β was varied from 22 to 90, implying super-

criticalities, $\bar{U}\lambda_1^2\beta^{-1}$, which ranged from 1.4 to 6.7. The results in this case are broadly similar to those of the constant β simulations. Note that the choices for the fit parameters γ and $\gamma\Delta$ were not changed from those chosen from the first set of runs. Notably, the variation in the predicted slopes for \hat{V}_1 differ more with β than with \bar{U} and, at least in the small β (strongly unstable) regime, the simulation results fall very close to the slope predicted by the constant Δ scaling.

c. Sensitivity to stratification scale depth

Figures 2 and 4 both demonstrate that the power law slopes of the steady-state statistics are nearly the same for the two stratification profiles considered, but also show that the barotropic energy is lower in the nonuniform stratification case than in the uniform case. The main difference between a system with uniform and nonuniform stratification is the presence of baroclinic self-advection in the latter (Fu and Flierl 1980; SV), which formally weakens the passive scalar analogy to baroclinic flow. Considering the two-mode equations written in the form (3.1), any difference in the dynamics between systems with uniform and nonuniform strati-

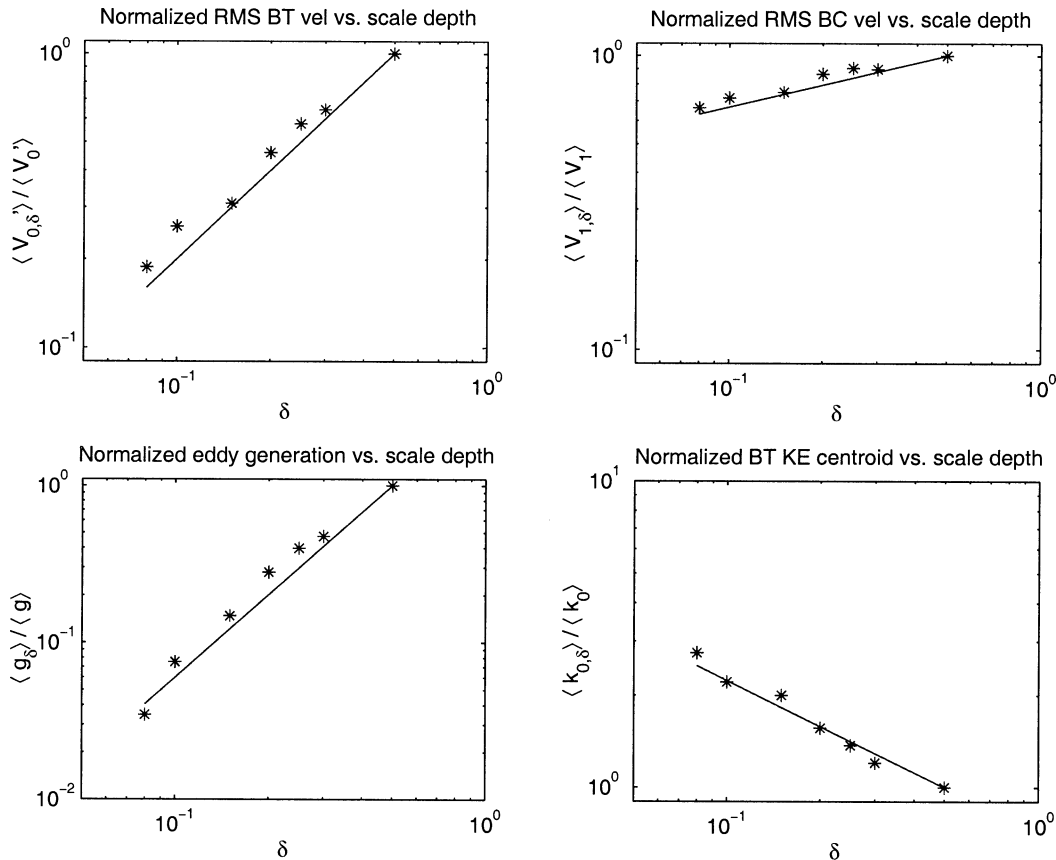


FIG. 5. Statistics from sequence of 5 layer by 256^2 simulations in which the exponential stratification scale-depth δ is varied between from 0.08 to linear (corresponding to 0.5). The mean zonal shear projects only onto the first baroclinic mode with the value $\bar{U} = 0.1$. The first baroclinic deformation wavenumber is held fixed at $\lambda_1 = 35$ (by varying the effective domain size) and the Coriolis gradient is $\beta = 50$, hence the supercriticality is fixed at $\bar{U}\lambda_1^2\beta^{-1} = 2.5$ (although the actual wavenumber of maximum growth and the growth rate itself vary with δ in the linear stability calculation). The drag is $r = 0.2$. Layout is just as for Fig. 2 except that for each statistic the data have been normalized by their values for the linear density profile ($\delta = 0.5$). The actual values for the linear profiles are $\langle V'_0 \rangle = 1.7$, $\langle V'_1 \rangle = 0.22$, $g = 0.23$, and $K_0 = 4.8$. The solid lines for the rms eddy velocities are empirical fits (by eye), corresponding to 2δ for the barotropic velocity scale and $(2\delta)^{1/4}$ for the baroclinic velocity scale. The slopes for the eddy generation rate and stopping scale are derived from the former two, and correspond to $(2\delta)^{7/8}$ and $(2\delta)^{-1/2}$, respectively.

fication must be due to the terms multiplied by the interaction coefficient ξ , and the two such terms present always appear in sum as $\Psi'_0 + \xi\Psi'_1$. Because ξ is $O(1)$ (its largest value for any interaction in any of the simulations considered in this paper does not exceed 3), only at scales K^{-1} such that $\langle \Psi'_1 \rangle_K \sim \langle \Psi'_0 \rangle_K$ will terms multiplied by ξ be important. An a posteriori analysis confirms that this is only true at scales of order or smaller than the deformation scale. One can find evidence for this claim in Fig. 3. The available potential energy in the first baroclinic mode is $A_1 = \lambda^2 |\Psi_1|^2 / 2$ while the barotropic kinetic energy is $T_0 = K^2 |\Psi_0|^2 / 2$. Therefore $\tilde{\Psi}_0 \approx \sqrt{2T_0/K^2}$ and $\tilde{\Psi}_1 \approx \sqrt{2A_1/\lambda^2}$. At large scale, the spectra of $A_1 \ll T_0$, thus $\langle \Psi_1 \rangle_{K \ll \lambda} \ll \langle \Psi_0 \rangle_{K \ll \lambda}$. The scaling arguments, then, which rely upon the treatment of the baroclinic mode as a passive scalar at large scale, should (and do) apply independent of stratification type. Nevertheless, processes occurring near the deformation

scale affect the transfers between modes, and the degree to which the ξ terms (which may be significant at these scales) affect transfers in the forced-dissipative dynamics is not obvious.

A series of simulations was performed in which the scale depth δ was varied while holding the other parameters fixed. Results are shown in Fig. 5. We find that the barotropic eddy velocity scale varies as $\tilde{V}_0 \propto \delta$ (see figure) while the baroclinic eddy velocity is relatively insensitive to the scale-depth (varying as $\tilde{V}_1 \propto \delta^{1/4}$). SV showed that the baroclinic self-interaction coefficient [see (3.1)] $\xi \propto \delta^{-1/2}$, where δ is the scale depth of the stratification. However, we have no definitive scaling analysis that explains the quantitative statistical dependence upon δ observed in the present case, so we accept the observed dependence as an empirical scaling law. In qualitative terms, one can infer from the results that the stratification terms [those multiplied by ξ in (3.1)]

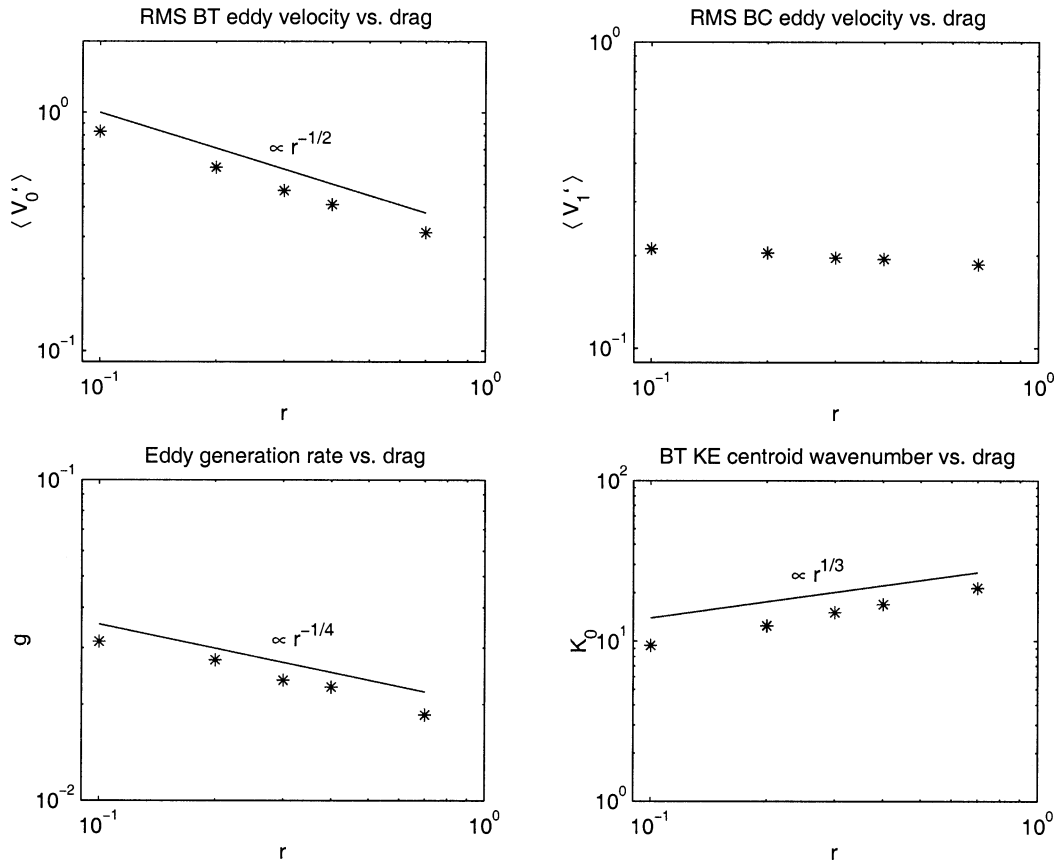


FIG. 6. Statistics from sequence of 5 layer by 128^2 simulations in which the bottom drag r is varied from 0.1 to 0.7. The mean zonal shear projects only onto the first baroclinic mode with the value $\bar{U} = 0.16$, and $\beta = 50$ and $\lambda_1 = 35$, so the supercriticality is $\bar{U}\lambda_1^2\beta^{-1} = 3.9$. A nondimensional measure of the drag is $r(\bar{U}\lambda_1)^{-1}$, which ranges from 0.018 to 0.13 here. Stratification is exponential with scale depth $\delta = 0.15$. Layout is just as for Fig. 2. Statistics from simulations are plotted as asterisks, and the solid lines represent slopes that, by eye, approximate the power law scaling of the statistics.

act to inhibit transfers to the barotropic mode, thus lowering the barotropic eddy energy level, which in turn reduces the eddy generation rate by just the amount necessary to keep the baroclinic kinetic energy level nearly constant.

The empirical dependence of \tilde{V}_0 and \tilde{V}_1 on δ can be used to modify the scalings (3.11), thereby allowing us to glean the concurrent dependence of the stopping scale and generation rate on δ . In Fig. 5 we observe that

$$\frac{\tilde{V}_{0,\delta}}{\tilde{V}_0} \approx 2\delta \quad \text{and} \quad (4.6)$$

$$\frac{\tilde{V}_{1,\delta}}{\tilde{V}_1} \approx (2\delta)^{1/4}, \quad (4.7)$$

where $\tilde{V}_{0,\delta}$ and $\tilde{V}_{1,\delta}$ are the rms velocity scales for simulations in which the stratification is nonuniform (with scale-depth δ), and we assume that \tilde{V}_0 is given in (3.11a). Since the stopping scale K_0 is given by (3.5) and the generation rate g by (3.8), we can again use (4.6) and (4.7) to write

$$K_{0,\delta} \approx (2\delta)^{-1/2}K_0, \quad g_\delta \approx (2\delta)^{7/8}g. \quad (4.8)$$

[We have been imprecise by using a fit for \tilde{V}_1 in the place of \hat{V}_1 where it appears in (3.8), but the result is ultimately empirical, so more care is not necessary.] The dashed lines in Figs. 2 and 4 were calculated by using the expression for \tilde{V}_0 (3.22a) in (4.6) and (4.8).

d. Sensitivity to bottom drag

The heuristic picture adopted assumes that β halts the cascade and that, although bottom drag must ultimately dissipate the energy fluxing through the system, it does not affect the halting scale of the inverse cascade (see appendix A). That this should be so is not obvious, and in this section a set of runs is described in which all other parameters are held fixed while the bottom drag is varied. In the theory developed so far, no dependencies upon the bottom drag r have been suggested, despite that it is the primary mechanism by which energy is removed from the system. Figure 6 demonstrates that there is, in fact, a dependence of the eddy statistics on

bottom drag, but that this dependence is weak. The baroclinic eddy velocities are nearly insensitive to drag and the most sensitive dependence is in the barotropic eddy velocity, which scales as $\tilde{V}_0 \sim r^{-1/2}$ —still weak compared to the dependence on β and \bar{U} found in sections 4a and 4b.

It should be pointed out that all of the values considered (in the range $r \in [0.1, 1]$) are in a “small drag” regime—specifically as compared to typical values of the inverse eddy timescale $T_e^{-1} = \bar{U}\lambda$. This, however, is likely the relevant range for oceanic applications, in which typical inverse spindown times are of order $r = 10^{-6}$ – 10^{-7} s^{-1} . Estimating $\bar{U} \sim 0.1 \text{ m s}^{-1}$ and $\lambda \sim 2\pi/(100 \text{ km})$, indeed $r \ll T_e^{-1}$, and the small drag range is appropriate.

e. A test of the passive scalar approximation to baroclinic flow

In this last subsection we discuss a set of simulations designed to investigate the passive scalar approximation to baroclinic dynamics. A set of two-layer simulations was performed with the addition of a concurrently integrated passive scalar *advected by the barotropic mode* and forced by a mean gradient. Specifically, we integrated

$$\frac{\partial \tau}{\partial t} + J(\Psi_0, \tau - \bar{U}y) = \lambda^{-2} \nu \nabla^8 \tau, \quad (4.9)$$

where $\tau = \tau(x, y, t)$ is the passive scalar and \bar{U} is the baroclinic mean shear that forces the flow. In essence (4.9) is just (3.2)—the expected form of the baroclinic mode in the two-mode case at large scale. Four simulations were performed between which the mean shear was varied. Each of the simulations used the values $\lambda = 50$, $\beta = 50$, and $r = 0.2$, while the mean shear \bar{U} was given the values $0.07, 0.1, 0.12, 0.14$, corresponding to supercriticalities $\bar{U}\lambda^2\beta^{-1} = 3.5, 5.0, 6.0, 7.0$. In Fig. 7 the baroclinic kinetic energy spectra for each run are plotted along with the analogous “tracer kinetic energy,” $K^2 |\tau|^2$. At large scale the two spectra are nearly identical, and in particular the values of the spectra at the barotropic stopping wavenumber K_0 (which is different for each simulation) are nearly the same for both fields. In the lower panel of Fig. 7 the statistic $\hat{V}_\tau = [2K_0^2 |\tau_{K_0}|^2]^{1/2}$ (analogous to the mixing-scale baroclinic rms eddy velocity \hat{V}_1) is plotted as a function of \bar{U} , alongside lines whose slopes correspond to the predictions of turbulent diffusion ($\hat{V}_\tau \propto \bar{U}$) and constant Δ ($\hat{V}_\tau \propto \bar{U}^3$).

At the smaller values of \bar{U} , that is, in the more weakly unstable simulations, the behavior is perhaps best described by turbulent diffusion, while in the more strongly unstable simulations it clearly is not. These results imply that even strict scalar dynamics, when stirred by finite resolution, β -halted barotropic flow, do not conform to the behavior expected from turbulent diffusion. Thus the divergence from turbulent diffusive behavior

seen in the more complex five-layer simulations described in the previous subsections need be related neither to the presence of higher baroclinic modes nor to the presence of baroclinic self-advection terms resulting from nonuniform stratification. Rather, either finite resolution or the geometric effect of β may be responsible for the deviation from classical diffusive behavior.

A possible explanation follows. As the forcing becomes stronger, the energetic peak moves closer to the domain scale, leaving less room for the peak to spread in width, thus fixing Δ . On the other hand, as the forcing becomes weaker, the peak moves closer to the deformation scale, reducing or removing the inertial range upon which the diffusive arguments rely. This explanation is consistent with results from simulations in which only the third baroclinic mode is forced (to be discussed in section 6)—in this case, the relevant deformation scale is much smaller, leaving a significant spectral range within which to vary the stopping scale without approaching the domain scale. Classic turbulent diffusive behavior is, indeed, observed when only higher baroclinic modes are forced.

5. Steady-state statistics and vertical structure in the fully stratified case

When the mean shear primarily reflects the first baroclinic mode, the two-mode limit seems to provide a semiquantitative description of the fully stratified system. However, the structure of the mean shear need not project only onto the first baroclinic mode, and we would like to understand the dynamics of the case with arbitrary vertical shear.

a. Eddy statistics with arbitrary shear

The theoretical ideas of section 3 can be applied to the general case. From appendix B one has an expression for the eddy generation due to arbitrary shear

$$g \approx \sum_m \bar{U}_m \lambda_m^2 \overline{V'_m \Psi'_0}, \quad (5.1)$$

the generalization of the two-mode generation rate (3.7).

Conceptually, generation of baroclinic eddy energy will occur in those vertical modes onto which the shear projects, and at a horizontal scale where the barotropic energy accumulates (since generation is still driven by correlations with the barotropic streamfunction). In a given mode m , baroclinic kinetic energy will cascade downscale (by analogy with a passive tracer for that mode) until it reaches that mode’s deformation wavenumber, λ_m . At small horizontal scales, energy cascades, as in two-dimensional turbulence, upscale. Thus we expect energy in mode m to move toward its respective deformation scale. SV demonstrated that such energy then cascades either directly into the barotropic mode (in the uniformly stratified case) or to the first baroclinic mode (in the nonuniformly stratified case), where it then

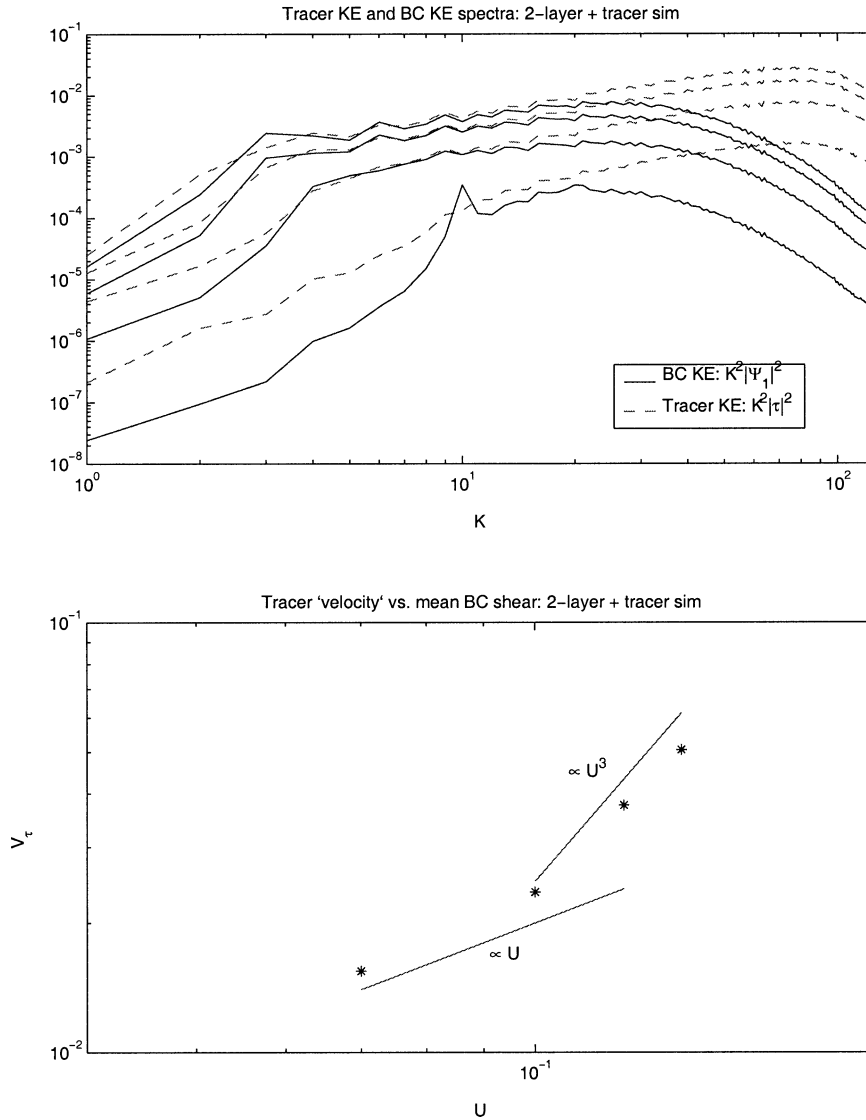


FIG. 7. Statistics from sequence of 2 layer by 256^2 simulations in which a tracer, advected by the barotropic flow and forced by a large scale mean gradient equivalent to the mean shear, is concurrently integrated. The mean zonal shear \bar{U} is varied from 0.07 to 0.14, while all other parameters are kept constant, with values $\beta = 50$, $r = 0.2$, and $\lambda = 50$. These values correspond to supercriticalities $\bar{U}\lambda_1\beta^{-1} = 3.5, 5.0, 6.7, 7.0$. The upper plot shows the baroclinic kinetic energy from each run alongside the analogous “tracer kinetic energy” ($K^2|\tau|^2$) spectra. The lower panel shows estimations of the rms tracer “velocity” near the respective stopping scales K_0 : $\hat{V}_\tau = (2K_0^2|\tau_{K_0}|^2)^{1/2}$. The two solid lines in the lower plots correspond to the slopes predicted by classic turbulent diffusion ($\propto\bar{U}$) and by the constant Δ theory ($\propto\bar{U}^3$).

cascades toward the first baroclinic deformation scale, and finally into the barotropic mode. The barotropic eddy scales are then controlled (in the zonal flow, small-drag limits considered in this paper) by β , and the energy is ultimately removed by drag. Schema of this conceptual picture are shown in Fig. 8.

Quantitatively, the arguments that led to the Rhines scale (3.5) and the relation between the spectral flux and rms barotropic velocity (3.9) are valid in the fully stratified case if in the two-mode case, hence using (5.1)

one can solve for the rms barotropic velocity (\tilde{V}_0), the stopping scale (K_0), and the eddy generation rate (g) now in terms of the rms baroclinic eddy velocities for each mode in the neighborhood of the barotropic energy containing scale ($\langle V_m' \rangle_{K_0} \equiv \tilde{V}_m$). The results are

$$\begin{aligned}\tilde{V}_0 &\approx \alpha T_e^{-2} \beta^{-1}, & K_0 &\approx \alpha^{-1/2} T_e \beta, \\ g &\approx \alpha^{3/2} T_e^{-5} \beta^{-2},\end{aligned}\quad (5.2)$$

where

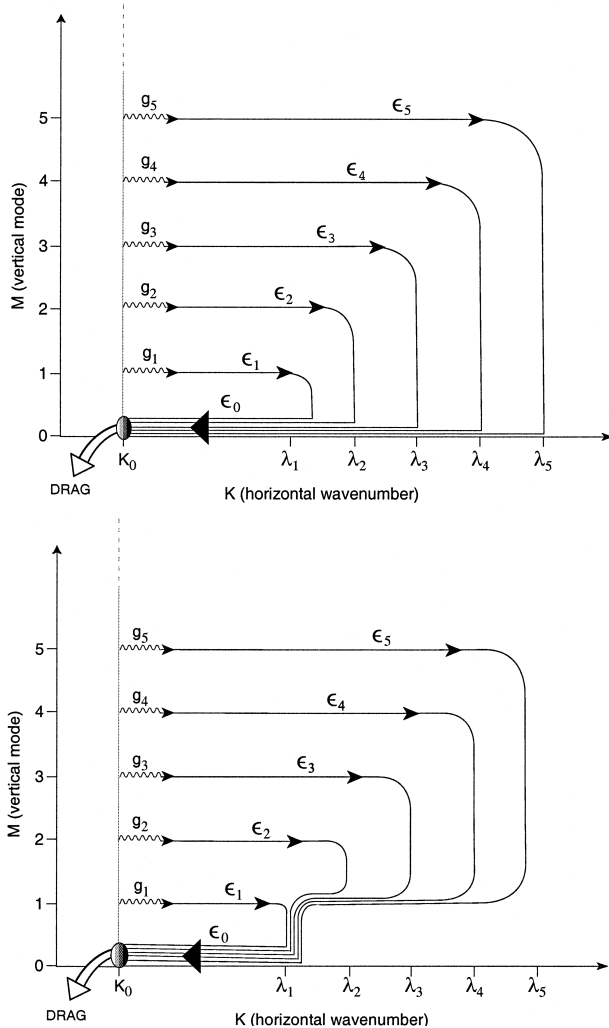


FIG. 8. Upper panel: conceptual schematic of energy transfers in uniformly stratified system. The mean shear projects onto the mean stratification such as to give generations g_m into each mode m . The energy is then, approximately, transferred (ϵ_m) downscale first to the deformation wavenumber of that mode, and then to the barotropic mode. Lower panel: a similar schematic for a system with surface-intensified stratification. In fact, in both cases transfers from higher modes are not as localized in horizontal wavenumber as is drawn, and there is significant transfer to the graver vertical modes at wavenumbers lower than the deformation wavenumber of the higher vertical mode.

$$T_e^{-2} \equiv \sum_m \bar{U}_m \lambda_m^2 \tilde{V}_m \quad (5.3)$$

is the squared inverse eddy timescale for the fully stratified system [compare to T_e^{-2} in (3.21)].

One is again left with the problem of estimating the baroclinic eddy velocities \tilde{V}_m , but the problem is now more complicated. The difficulty in proceeding, as in the two-mode case, by integrating presumed spectra for the baroclinic eddy kinetic energies is the lack of advance estimates for the individual baroclinic spectral fluxes ϵ_m or generation rates g_m . One might suppose that

the individual terms in the sum over modes in the expression for g (5.1) could be used, but this leads to a degenerate result. Hence for the higher mode scaling, at least when more than one mode is forced, we make the assumption of classic turbulent diffusion, in which case one can say simply $\tilde{V}_m \approx a \bar{U}_m$, where a is an undetermined proportionality constant [in terms of (3.20), $a = \gamma/\alpha$], so that

$$T_e^{-2} \equiv a \sum_m \bar{U}_m^2 \lambda_m^2. \quad (5.4)$$

This expression for the eddy timescale is the modal equivalent to Eq. (27) of HL (apart from the factor a).

We have not explicitly included any scaling dependence upon the stratification scale thickness δ . One could proceed again using the semiempirical results of section 4c as in (4.6) and (4.8), but given the growing number of assumptions in the present, more complex case, this may be premature.

b. Vertical structure of the horizontal eddy potential vorticity flux

The theory for the energy levels and horizontal scales of eddies is not sufficient to explain the vertical structure of eddy fluxes. Specifically one must also specify the vertical structure of $\overline{v'q'}$, and to this end we now consider the potential vorticity flux in terms of vertical modes.

First notice that the potential vorticity flux is given by the divergence of the Eliassen–Palm flux vector

$$\overline{v'q'} = \frac{\partial}{\partial z} \left(\frac{f_0^2}{N^2} \overline{v' \frac{\partial \psi'}{\partial z}} \right), \quad (5.5)$$

where the zonal divergence of momentum term does not appear since we are considering the horizontally homogeneous limit. Since we further assume a rigid lid and flat bottom, there are no surface buoyancy fluxes, and thus we have the constraint

$$\int_{-H}^0 \overline{v'q'} dz = 0. \quad (5.6)$$

Note that in the transformed Eulerian mean, the above meridional eddy potential vorticity flux is a forcing term to the mean zonal momentum, hence the constraint (5.6) is necessary in order for momentum to be conserved.

Representing the fields in terms of vertical modes, the meridional flux of potential vorticity is given by

$$\overline{v'q'} = \sum_{m,n=0}^{\infty} \phi_n(z) \phi_m(z) \overline{V'_m Q'_n}. \quad (5.7)$$

The arguments and derivations in appendix B lead us to conclude that the dominant contribution to this is given by

$$\overline{v'q'} \approx \sum_{m=1}^N \phi_m(z) \overline{V'_0 Q'_m}. \quad (5.8)$$

The scaling relations derived in the previous section can now be used to estimate this flux. Proceeding in the manner that led to the estimate of the eddy generation rate (3.8), one can estimate $\overline{V'_0 Q'_m} \approx \langle V'_0 \rangle \langle Q'_m \rangle_{k_0}$. Using the estimate (B.8) for baroclinic rms eddy potential vorticity, the relations (5.2) and the presumption $\hat{V}_m \approx a\overline{U}_m$, we have

$$\overline{V'_0 Q'_m} \approx \alpha^{3/2} a \overline{U}_m \lambda_m^2 T_e^{-3} \beta^{-2}, \quad (5.9)$$

where T_e is given by (5.4).

Combining (5.8) and (5.9) gives

$$\overline{v'q'} \approx \alpha^{3/2} a T_e^{-3} \beta^{-2} \sum_{m=1}^N \overline{U}_m \lambda_m^2 \phi_m(z) = DS(z), \quad (5.10)$$

where $D = \alpha^{3/2} a T_e^{-3} \beta^{-2}$ is the predicted diffusivity and

$$S(z) = \sum_{m=1}^N \overline{U}_m \lambda_m^2 \phi_m(z) = -\frac{d}{dz} \left(\frac{f^2}{N^2} \frac{d\bar{u}}{dz} \right), \quad (5.11)$$

where (2.4) and (2.12) have been used. In the strongly unstable limit ($\beta \ll \overline{U}_m \lambda_m^2, \forall m > 0$), the mean potential vorticity gradient $\partial \bar{q} / \partial y \approx S(z)$. Thus, we have down-gradient flux of eddy potential vorticity in the limit of small β .

Equation (5.10) specifies an eddy parameterization, applicable in the limits of highly unstable flow and negligible momentum transport (consistent with the horizontally homogeneous limit). The suggested parameterization has the advantageous property that (5.6) is automatically satisfied independent of the choice of scaling parameters since (5.8) is a linear sum of modes, each of which vanishes independently upon integration in z . Green (1970) and White and Green (1984) presented an eddy parameterization scheme in which integrated momentum is ensured by specifying the vertical structure of the eddy transport (Austausch) coefficients in a particular way. In our scheme the required conservation properties fall out naturally, although we do not consider momentum transport. Also, the present theory does not include the effects of surface buoyancy fluxes, which add a nonzero term to the right-hand side of (5.6).

6. Simulations with higher baroclinic mode forcing

a. Forcing a single higher mode

We now consider a set of cases in which the mean zonal shear projects onto a single higher ($m > 1$) baroclinic mode. In particular we will describe 5 layer by 256^2 equivalent horizontal gridpoint simulations in which $\overline{U}(z)$ projects exactly onto the third baroclinic mode, that is, such that $\overline{U}_m = 0, \forall m \neq 3$. The single nonzero component (\overline{U}_3) is varied systematically to investigate the eddy statistics. We use the same vertical structure as in the nonuniform stratification runs described in section 4, exponential with scale depth $\delta = 0.15$ and $\lambda_1 = 35$. The higher mode deformation wavenumbers are thus $\lambda_2 = 71.5, \lambda_3 = 102$, and $\lambda_4 = 108$.

In the spectral calculation we resolve motions up to wavenumber $K_{\max} = 127$, thus capturing all deformation wavenumbers. The bottom drag is set to $r = 0.4$ for these runs, and $\beta = 50$. The values of shear used were $\overline{U}_3 = 0.01$ to 0.05 , corresponding to supercriticalities $\overline{U}_3 \lambda_3^3 \beta^{-1} = 2.1$ to 10.4 .

The same set of statistics plotted for the case in which the first baroclinic mode was forced are plotted for the present sequence of simulations in Fig. 9. The two theory lines represent (3.22) and (3.20) with $\overline{U} = \overline{U}_3, \lambda = \lambda_3$. Again, the same fit parameter derived for the statistics shown in Fig. 2 is used. The striking result is that, in contrast to the cases in which the first mode was forced, the turbulent diffusion assumption now seems to describe the data with greater accuracy than the constant Δ theory. One possible explanation is the following: each higher mode has a successively smaller baroclinic deformation scale so that motions near the barotropic halting scale K_0 increasingly (with higher mode m) satisfy the condition $K_0 \ll \lambda_m$, necessary in order to make the passive scalar analogy for motions in mode m (see discussion at the end of section 4e).

In Fig. 10 we show the spectra of kinetic energy for each mode in the central run of the sequence ($\overline{U}_3 = 0.03$). One can see that the barotropic mode energy dominates, but also that, despite the forcing of the third baroclinic mode, the bulk of the baroclinic kinetic energy lies in the first baroclinic mode, in accord with the expectations of SV. While this prominence of the first baroclinic mode was foretold, the qualitative picture described in SV gives no guidance in quantitatively modifying the scaling theories to include said effect. The spectral slopes of the barotropic kinetic, first baroclinic potential (not shown) energy, as well as for the kinetic energy of the forced baroclinic mode, are similar to those in Fig. 3 (where the forced mode is the first mode in that figure and the third mode in the present case).

We shall also consider the magnitude and vertical structure of potential vorticity fluxes for these five simulations. Assuming that a single higher mode m is forced and that baroclinic eddy velocities are given by (3.20d), the potential vorticity flux (5.10) becomes

$$\overline{v'q'} \approx \alpha^{-1} \gamma^{5/2} \overline{U}_m^4 \lambda_m^5 \beta^{-2} \phi_m(z). \quad (6.1)$$

In the top panel of Fig. 11 we show $\overline{v'q'}(z)$ from one of the simulations ($\overline{U}_3 = 0.03$, the same simulation as that for which the spectra are shown in Fig. 10) along side the prediction from (6.1), but multiplied by 3 in order to fit the simulation in magnitude. Note that the shape of the theory curve is thus exactly that of the third baroclinic mode $\phi_3(z)$. The maxima for all five simulations are plotted in the lower panel of Fig. 11 and compared to the prediction from (6.1), using, again, the same fit parameter γ derived for the first set of simulations discussed. Also shown in theory multiplied by 3, which yields a better fit to the results. In all cases the theory seems to do reasonably well in predicting the structure and scaling of the fluxes [despite that we have

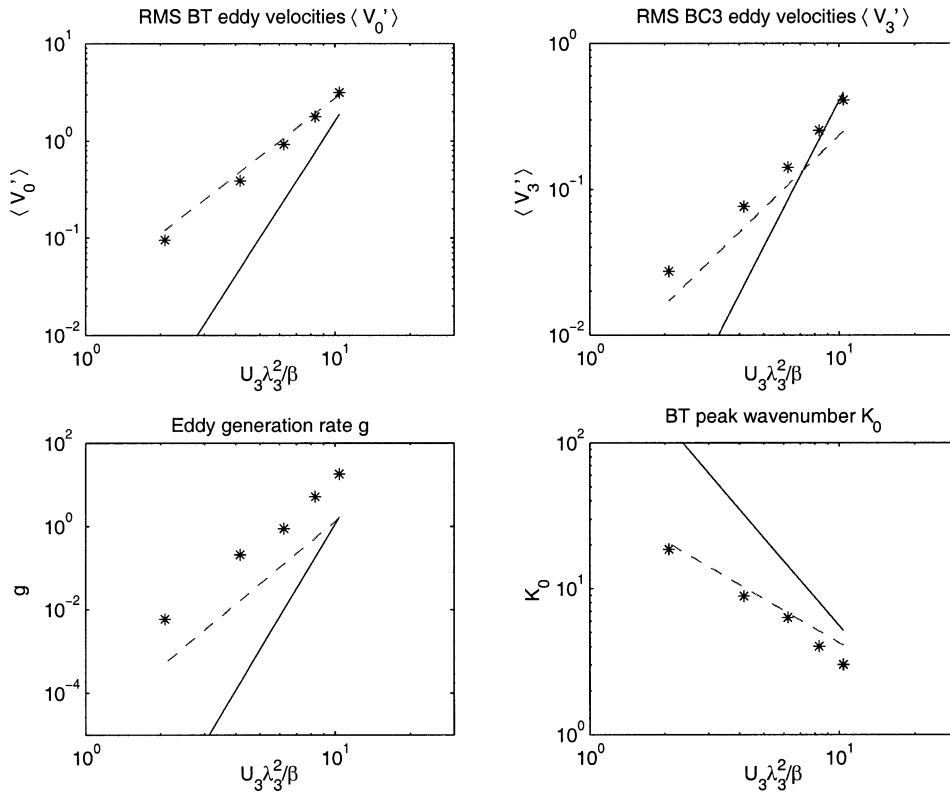


FIG. 9. Statistics from sequence of 5 layer by 256^2 simulations in which the amplitude of the mean third mode baroclinic shear is varied between $\bar{U}_3 = 0.01$ and 0.05 . The mean zonal shear projects only onto the third mode, $\beta = 50$ and $r = 0.4$. Statistics are plotted against a measure of the supercriticality for these runs, $\bar{U}_3 \lambda_3^2 \beta^{-1}$, which ranges from 2.1 to 10.4. All of these runs have surface intensified stratification with scale depth $\delta = 0.15$. Layout is as in Fig. 2.

not accounted for the extra energy in the (unforced) first baroclinic mode], but underpredicts the magnitude by a factor of 3.

b. Forcing with realistic shear

In order to test the full theory, we performed a simulation with 15 layers, 256^2 equivalent horizontal grid points, and semirealistic profiles of stratification and mean zonal shear to statistical steady state. The profiles, shown in Fig. 12, are slightly smoothed interpolations from the shear and potential density profiles generated by a primitive equation simulation of the North Atlantic at some midlatitude location away from horizontal boundaries (the first few modes of the stratification are shown in Fig. 13). The density profile is no longer a simple exponential form and the mean shear does not project onto any one mode alone. As with the other simulations, $\beta = 50$ and $r = 0.2$.

The upper panel of Fig. 14 shows supercriticalities $\bar{U}_m \lambda_m^2 \beta^{-1}$ for each mode separately. By this measure, most of the instability of the flow is generated in the first few modes, with a peak in mode 3, but also at the highest mode, 14. The lower panel of Fig. 14 shows the baroclinic eddy velocities (near the stopping scale) \hat{V}_m

versus mode m on a log scale. Also shown are the projections of the mean shear onto the modes (\bar{U}_m), multiplied by a scale factor ($a = 0.25$). The degree to which these two coincide represents the degree to which higher mode baroclinic potential vorticities can be described as being turbulently diffused by the barotropic flow. One should note in particular the variations from this fit for the first few modes, which are likely the most important. Note especially that the $\hat{V}_1 / \hat{V}_2 > \bar{U}_1 / \bar{U}_2$, while $\hat{V}_2 / \hat{V}_3 \approx \bar{U}_2 / \bar{U}_3$, consistent with the expectation of extra energy in the first baroclinic mode.

In Fig. 15 we plot $\overline{v'q'}(z)$ with depth along with a curve whose shape is that of (5.10), but whose magnitude has been rescaled to fit the results. Specifically, we discard the nondimensional factors in the theory and plot

$$\overline{v'q'}_{\text{THEORY}} = 0.1 \times T_e^{-3} \beta^{-2} \sum_{m=1}^N \bar{U}_m \lambda_m^2 \phi_m(z).$$

The shape of the flux is, notably, not captured by any single mode (compare with curves in Fig. 13). In an eddy parameterization scheme, one should expect an overall nondimensional tuning factor to be determined empirically. The results for cases with single mode forc-

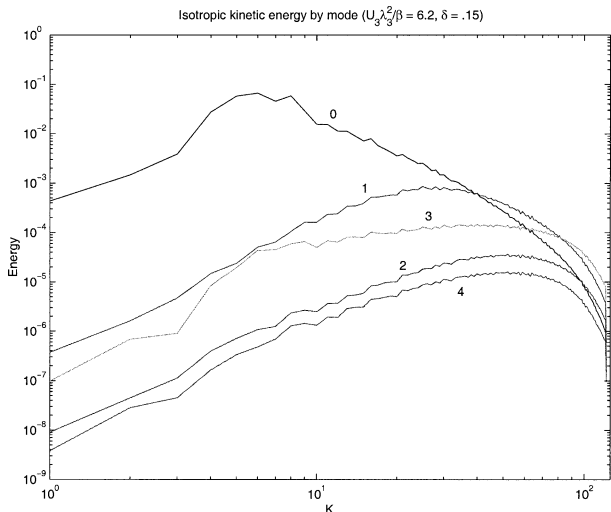


FIG. 10. Spectra of kinetic energy by mode for central run ($\bar{U} = 0.03$) in sequence of simulations for which statistics are shown in Fig. 9. Note that although only the third mode is forced, significant kinetic energy is concentrated in the first baroclinic mode near the first baroclinic deformation scale.

ing imply that this scaling factor for the diffusivity is independent of the flow, but an ensemble of runs similar to the present 15-layer run would need to be performed in order to verify that this remains true for more complicated mean flows.

In Fig. 16 we show the barotropic and first baroclinic kinetic energy spectra, along with the surface projection of the latter. As discussed in SV01 and pointed out by Wunsch (1997), surface-intensified stratification leads to surface-intensified baroclinic modes, and a consequent relative overrepresentation of baroclinic energy in the surface signal, possibly explaining part of the observed correlation of surface eddy scales with the first deformation scale.

7. Conclusions

We have focused here on the application of turbulence scaling theory to the statistics of eddies, such as those in the midlatitude oceans, forced by baroclinic instability of arbitrary zonal shears embedded in surface-intensified stratification. We find that one can, in the strongly unstable limit, predict the energy levels, scales, and structure of eddies as functions of the mean state, even when the mean state is rather complex.

The theory discussed builds on that of HL, which was derived based on a system with two equal-thickness layers (uniform stratification) and homogeneous flow. As it turns out, the relationships between the equilibrated statistics and mean flow parameters obey the same power laws in both uniformly and nonuniformly stratified cases when only the first baroclinic mode is forced. The lack of distinction between uniform and nonuniform stratification in the slopes of the statistics

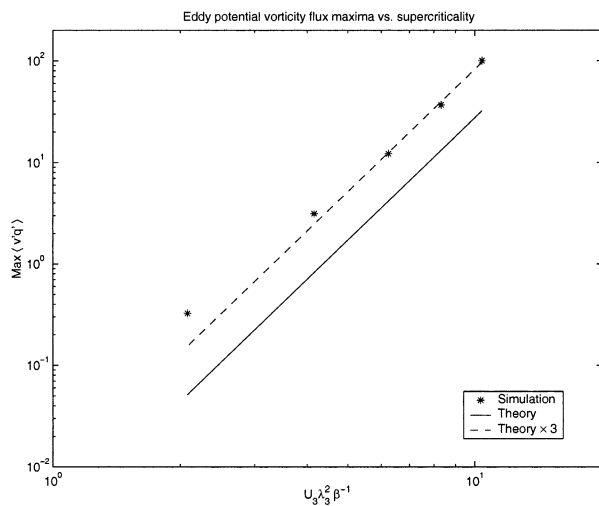
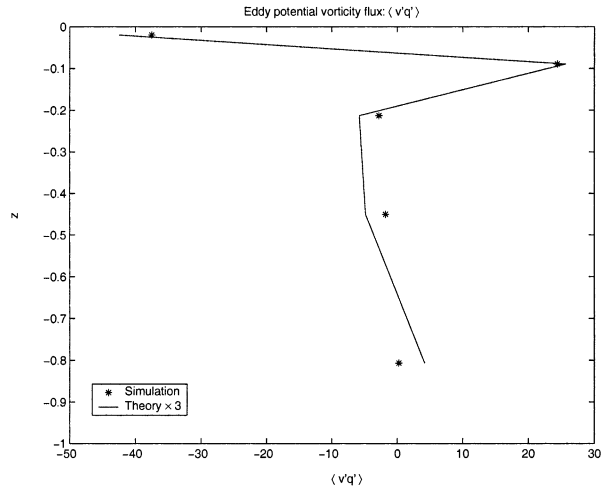


FIG. 11. Upper panel: meridional eddy potential vorticity flux versus depth for central run ($\bar{U} = 0.03$) in sequence of simulations whose statistics are shown in Fig. 9 (asterisks), and theoretical prediction for curve from (6.1) multiplied by a scale factor 3 (line). Lower panel: Maxima of meridional eddy potential vorticity flux vs supercriticality for same sequence of simulations (asterisks), and theoretical prediction for maxima from (6.1) (solid line), and same predictions multiplied by 3 (dashed line).

does not mean that the flow is unaffected by stratification. Rather, we find that the ratio of barotropic to baroclinic energy is reduced as the mean density profile is made increasingly surface intensified, yielding increasingly baroclinic flows in the presence of a strong pycnocline.

Although the power laws observed are independent of stratification scale depth, they are also different than those predicted by HL for the cases in which only the first baroclinic mode is forced. Held and Larichev assume that downgradient diffusion of potential vorticity implies that baroclinic velocity variances are proportional to the mean baroclinic shear. In fact, this scaling is not observed in the first mode forcing cases, despite that potential vorticity is diffused downgradient. A mod-

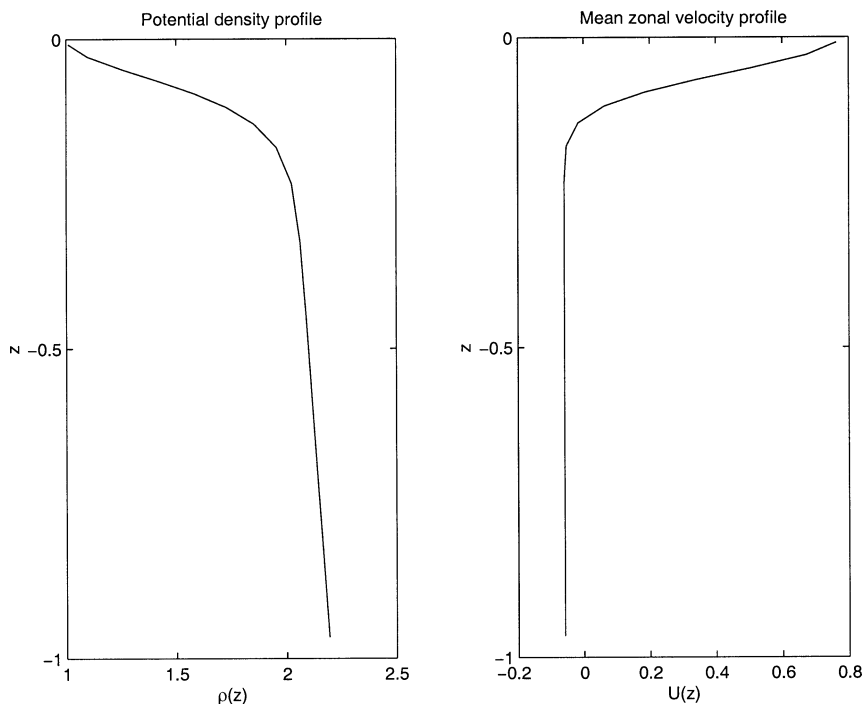


FIG. 12. Nondimensionalized profiles of mean potential density (left) and mean zonal velocity (right) with depth extrapolated from a simulation of the North Atlantic (strongly restored toward climatology). These profiles are used in the 15 layer by 256^2 run discussed in section 6b.

ification was proposed that gives the correct scalings, but introduces an undetermined length scale. The scaling of the baroclinic velocity is related to the treatment of the baroclinic streamfunction as a passive scalar. Tests in which a true passive scalar is advected by the barotropic mode of an unstable two-layer flow demonstrate that the underlying cause of the revised scaling is present even in that simpler case. We expect that the undetermined length scale is related to the finite domain size in the simulations.

That finite domain size modifications to turbulent diffusion might cause the deviant scaling of the passive scalar flux is consistent with the observation that when only higher baroclinic modes are forced, the baroclinic velocity variance *does scale* like the mean baroclinic shear for that forced mode. Hence ultimately, we expect that this scaling is appropriate for baroclinic dynamics in the ocean, at least in regions of strongly unstable flow.

As in SV, our exploration of the fully stratified case takes advantage of the modal viewpoint, for various reasons. Foremost, in the homogeneous limit, the vertical structure of the turbulent dynamics is sensitive to scale, just as is the horizontal structure. We can, in some sense, “diagonalize” the inhomogeneous nature of the stratification and shear through the choice of stationary basis functions, the vertical modes of the stratification. One can only use these modes in the limit of slowly varying mean stratification and shear, but this is likely a reasonable approximation for the extratropical mid-ocean. The formal analogy between energy in baroclinic modes and passive scalar dynamics provides a second motivation for considering the modal projections of the motion. Moreover, each mode possesses a well-defined scale (its deformation scale) at which energy in that mode will tend to concentrate and at which transfers to lower modes occur.

The potential vorticity flux form (5.10) could form the basis for an eddy parameterization scheme in coarse

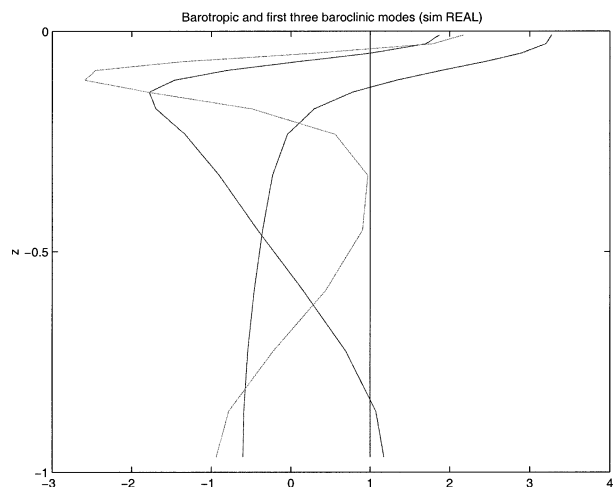


FIG. 13. Barotropic and first three baroclinic modes for density profiles shown in Fig. 12.

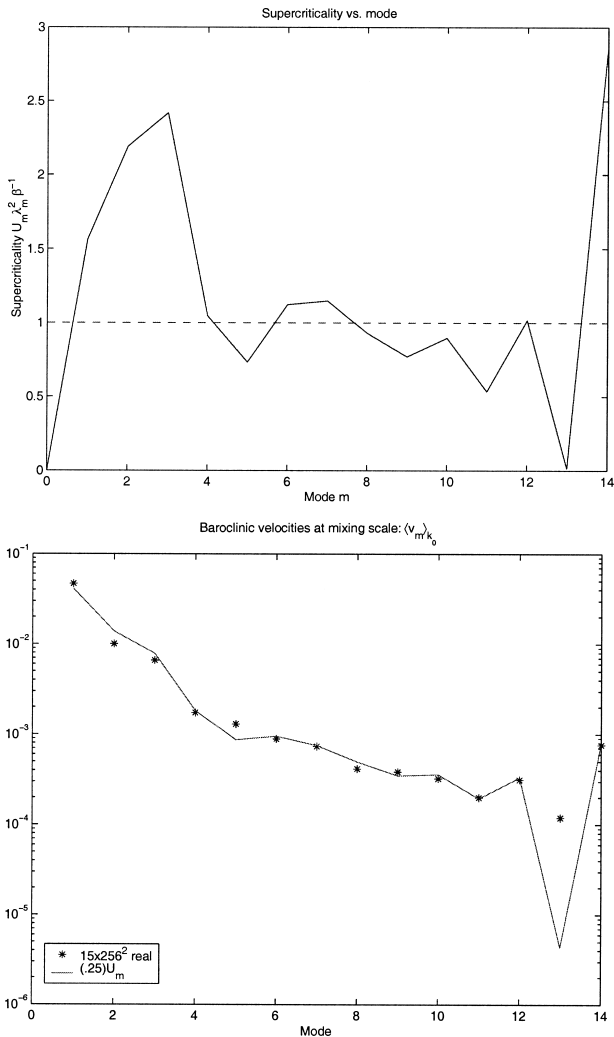


FIG. 14. (top) Supercriticalities $\overline{U}_m \lambda_m^2 \beta^{-1}$ for each mode separately. (bottom) Semilog plot of rms eddy velocities near the mixing scale $\langle v'_{m,k_0} \rangle$ for each baroclinic mode (asterisks) in 15 layer by 256^2 simulation with realistic shear and density profiles. Also shown is the theoretical prediction $\hat{V}_m \approx a \overline{U}_m$ (solid line).

resolution ocean models, with the advantage that its vertical structure is specified in a manner that is simple to calculate and that identically satisfies the imposed constraint that it vanish upon integration. [Wardle and Marshall (2000), for example, describe a possible method by which a potential vorticity diffusion closure could be incorporated into primitive equation ocean models, which in general do not prognose potential vorticity.] The formalism derived can straightforwardly be extended to nonzonal flows, using the ideas of Spall (2000), and possibly to include the effects of small-scale topographic roughness. Operationally, one could either periodically solve an eigenvalue problem for the stratification in a grid box to find the local neutral modes and deformation scales or calculate the shear and depth-dependent Richardson number. In as much as the mean

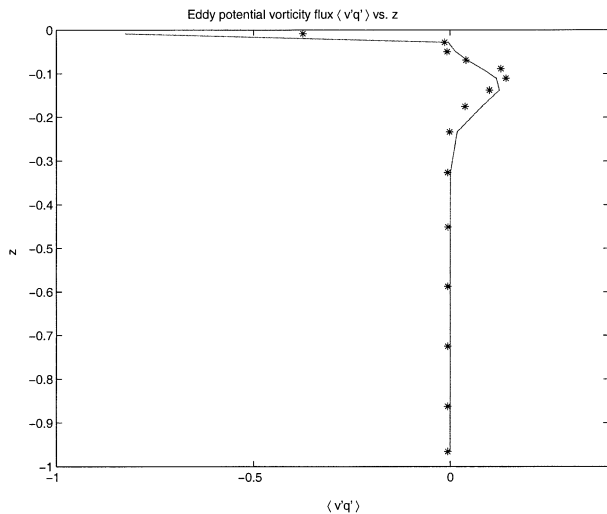


FIG. 15. Profile of northward eddy potential vorticity flux $\overline{v'q'}$ from 15 layer by 256^2 simulation (asterisks) compared to theory based on (5.10), but multiplied by an overall scale factor chosen to fit the simulation results. Specifically, the solid line is $0.17 T_e^{-3} \beta^{-2} \sum_{m=1}^N \overline{U}_m \lambda_m^2 \phi_m(z)$.

state is slowly varying, either would be done rather infrequently.

The proposed eddy flux theory also has some shortcomings. Momentum transfer is neglected, which may be important in the presence of horizontal inhomogeneity or strong barotropic shear; neither nonzonal effects nor surface buoyancy fluxes are accounted for; the reliance upon fixed vertical modes and quasigeostrophic dynamics precludes the ability to represent the effects on eddies of large-scale topography or strongly sloping isopycnals. At a more general level, the theory (like

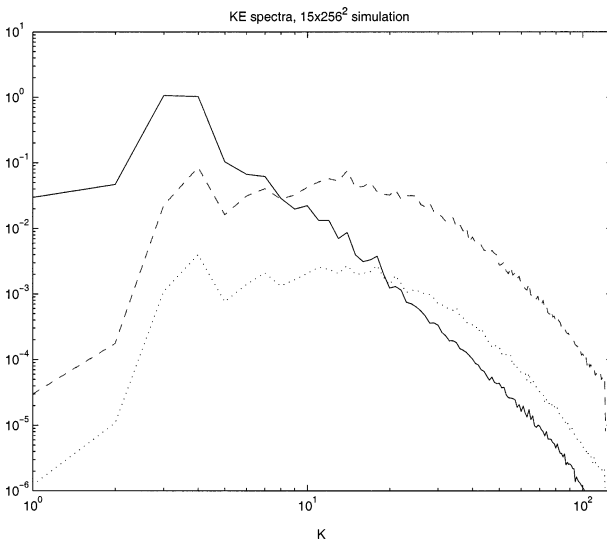


FIG. 16. Barotropic (solid line) and first baroclinic (dotted line) kinetic energy spectra for 15 layer by 256^2 simulation. Also shown is the relative projection of the first baroclinic energy in the uppermost layer (dashed line).

most diffusive theories) is *local*, in that the eddy transport is to be determined by the local properties of the background state, thus neglecting the possibly significant effects of eddy transport away from the location of eddy generation. Each of these missing effects is important in some area of the ocean. Nevertheless, given the scale separation between deformation-scale and basin-scale flow in the ocean, and given that eddy energy is so much larger than the energy of the time-mean flow, we feel that homogeneous geostrophic turbulence is the natural starting place for a theory of the scales, equilibration, and transport properties of eddies in the ocean.

Acknowledgments. The authors wish to thank Stephen Griffies, Isaac Held, and Bach-Lien Hua for very helpful discussions regarding this work. All simulations were performed on the supercomputers at NOAA's Geophysical Fluid Dynamics Laboratory. The work was also funded by the NSF under Grant OCE 0002295 and the ONR under Grant N00014-99-1-0211.

APPENDIX A

Cascade Halting

In general, we will assume that the cascade is halted at a scale such that the dispersion relation for a competing process yields a *faster* timescale than that of the nonlinear interactions which beget the turbulent cascade. Regardless of the mechanism, we assume an eddy timescale

$$\tau(K) \approx [E(K)K^3]^{-1/2}, \quad (\text{A.1})$$

where $E(K) \propto L^3/T^2$ is the spectral energy density at wavenumber K . We presume energy in the barotropic mode to behave as in two-dimensional turbulence, hence we expect $E(K) = C_0 \epsilon^{2/3} K^{-5/3}$, where $\epsilon \propto L^2/T^3$ is the spectral energy flux, which must be constant through the inertial range by definition thereof, and C_0 is the Kolmogorov constant (which we will neglect in the following discussion). Hence in terms of the spectral flux rate, the eddy time becomes

$$\tau(K) \approx \epsilon^{-1/3} K^{-2/3}. \quad (\text{A.2})$$

In the present model, the only mechanisms available that might halt the cascade are bottom drag r and the Coriolis gradient β . As an illustration of how this theory can fail, consider first the possibility that the former might set the stopping scale. Following the general prescription (Rhines 1975; Vallis and Maltrud 1993; HL), we assume that the cascade of turbulent kinetic energy in the barotropic mode cannot efficiently continue when the eddy timescale becomes comparable to the timescale of a competing process. The relevant timescale is $\tau_{\text{drag}} \approx r^{-1}$, and setting this equal to (A.2) gives us an expression for the equilibrated eddy scale

$$K_0^2 \approx r^3 \epsilon^{-1}. \quad (\text{A.3})$$

Because energy is conserved, $g = \epsilon$, and upon substitution of (3.8) into the above we arrive at a degenerate expression for K_0 ,

$$K_0^2 \approx \left(\frac{r}{\lambda(\overline{U\hat{V}}_1)^{1/2}} \right)^3 K_0^2. \quad (\text{A.4})$$

The damping timescale does not decrease sufficiently steeply at large scales, implying that *linear drag* cannot halt the *cascade*.

Nevertheless, tests with two equal depth layers and $\beta = 0$ (much like those of Larichev and Held 1995) demonstrate that bottom drag *does halt* the cascade, though only with much larger values than those used with any simulation in this paper (i.e., values that are no longer small compared to T_c^{-1} in 3.21).

By contrast, we can use the same method to derive the β -halting scale. The Rossby wave period (ignoring anisotropy) is $\tau_{\text{Rossby}} \approx K/\beta$ —setting this equal to τ in (A.2) then yields

$$K_0^5 \approx \beta^3 \epsilon^{-1}. \quad (\text{A.5})$$

Finally, again presuming that $g = \epsilon$, and using (3.8), we find

$$K_0 \approx \frac{\beta}{\lambda(\overline{U\hat{V}}_1)^{1/2}}. \quad (\text{A.6})$$

APPENDIX B

Modal Expansions for Generation and Potential Vorticity Flux

a. Modal eddy generation

Multiplying (2.8) by Ψ'_m and summing over modes, we find that the net eddy generation due to baroclinic instability of the mean zonal shear is

$$\begin{aligned} g &= - \sum_{ijm} \xi_{mij} \overline{U_i \Psi'_m} \frac{\partial}{\partial x} (\lambda_i^2 \Psi'_j + Q'_j) \\ &= \sum_{ijm} \xi_{mij} \overline{U_i} [(\lambda_i^2 - \lambda_j^2) \overline{V'_m \Psi'_j} + \overline{V'_m \nabla^2 \Psi'_j}], \end{aligned} \quad (\text{B.1})$$

where the overbar implies, as before, a horizontal spatial average. When the boundaries of Ψ'_m are periodic,

$$\overline{V'_m \Psi'_m} \equiv 0 \quad \text{and} \quad \overline{V'_m \nabla^2 \Psi'_m} \equiv 0.$$

Moreover, an integration by parts and application of Green's theorem when $m \neq j$ reveals that

$$\overline{V'_m \nabla^2 \Psi'_j} = -\overline{V'_j \nabla^2 \Psi'_m}.$$

Then, since ξ_{mij} is symmetric upon the interchange of two indices, the above terms cancel upon the full summation of (B.1), and we are left with

$$g = \sum_{i \neq j, m} \xi_{mij} \overline{U_i} (\lambda_i^2 - \lambda_j^2) \overline{V'_m \Psi'_j}. \quad (\text{B.2})$$

The triple interaction coefficient ξ also obeys the rela-

tion $\xi_{0ij} = \delta_{ij}$, so we further exclude $m = 0$ from the summation. So far the result is rigorous, and we now make the assumption that the term in the summation involving Ψ'_0 dominates in magnitude; that is, $\langle \Psi'_0 \rangle \gg \langle \Psi'_m \rangle$, $\forall m > 0$. Then since $j = 0$ we must have $i = m$, so that

$$g \approx \sum_m \overline{U}_m \lambda_m^2 \overline{V'_m \Psi'_0}. \quad (\text{B.3})$$

b. Modal potential vorticity flux

We can expand the velocity and potential vorticity fields in vertical modes

$$\overline{v'q'} = \sum_{m,n=0}^{\infty} \phi_n(z) \phi_m(z) \overline{V'_m Q'_n}. \quad (\text{B.4})$$

Since the modes ϕ_m are orthonormal [see (2.5)], only terms in which $m = n$ contribute to the vertical integral of (B.4), but as now shown, these terms vanish identically in the horizontally homogeneous limit.

Consider the flux of mode m potential vorticity ($Q'_m = \nabla^2 \Psi'_m - \lambda_m^2 \Psi'_m$) by mode m velocities

$$\begin{aligned} V'_m Q'_m &= \frac{1}{2} \frac{\partial V_m'^2}{\partial x} - V'_m \frac{\partial U'_m}{\partial y} - V'_m \lambda_m^2 \Psi'_m \\ &= \frac{1}{2} \frac{\partial V_m'^2}{\partial x} - \frac{\partial}{\partial y} (V'_m U'_m) + \frac{\partial V'_m}{\partial y} U'_m - V'_m \lambda_m^2 \Psi'_m \\ &= \frac{1}{2} \frac{\partial}{\partial x} \left(V_m'^2 - U_m'^2 - \lambda_m^2 \frac{\partial \Psi_m'^2}{\partial x} \right) - \frac{\partial}{\partial y} (V'_m U'_m), \end{aligned} \quad (\text{B.5})$$

where $\partial V'_m / \partial y = -\partial U'_m / \partial x$ and $V'_m = \partial \Psi'_m / \partial x$ have been used. Thus in the horizontally homogeneous case

$$\overline{V'_m Q'_m} = 0, \quad (\text{B.6})$$

separately for each mode m , ensuring that (5.6) is satisfied identically.

If only one baroclinic mode, m , has significant amplitude, then

$$\overline{v'q'} = \phi_m(z) [\overline{V'_m Q'_0} + \overline{V'_0 Q'_m}]. \quad (\text{B.7})$$

Consistent with arguments in section 3 we assume that $\tilde{V}_0 \gg \tilde{V}_m$. Moreover, in the strongly unstable limit, the rms eddy potential vorticity

$$\langle Q'_m \rangle_{K_0} \approx \lambda_m^2 \hat{V}_m / K_0, \quad (\text{B.8})$$

and $\langle Q'_0 \rangle_{K_0} \sim \overline{U}_m \lambda_m$, so assuming $\hat{V}_m \sim \overline{U}_m$, the ratio of two rms potential vorticities scales like

$$\frac{\langle Q'_m \rangle_{K_0}}{\langle Q'_0 \rangle_{K_0}} \sim \frac{\overline{U}_m \lambda_m^2}{\beta}, \quad (\text{B.9})$$

which must be larger than unity for baroclinic instability to occur. Thus we can safely neglect the first term on the right-hand side of (B.7) and assume that the barotropic advection of baroclinic potential vorticity dominates the flux.

REFERENCES

- Barnier, B., B. L. Hua, and C. L. Provost, 1991: On the catalytic role of high baroclinic modes in eddy-driven large-scale circulations. *J. Phys. Oceanogr.*, **21**, 976–997.
- Charney, J. G., 1971: Geostrophic turbulence. *J. Atmos. Sci.*, **28**, 1087–1095.
- Fu, L. L., and G. R. Flierl, 1980: Nonlinear energy and enstrophy transfers in a realistically stratified ocean. *Dyn. Atmos. Oceans*, **4**, 219–246.
- Gent, P. R., and J. C. McWilliams, 1990: Isopycnal mixing in ocean circulation models. *J. Phys. Oceanogr.*, **20**, 150–155.
- Green, J. S. A., 1970: Transfer properties of the large-scale eddies and the general circulation of the atmosphere. *Quart. J. Roy. Meteor. Soc.*, **96**, 157–185.
- Held, I. M., and V. D. Larichev, 1996: A scaling theory for horizontally homogeneous, baroclinically unstable flow on a beta-plane. *J. Atmos. Sci.*, **53**, 946–952.
- Holloway, G., 1986: Eddies, waves, circulation, and mixing: Statistical geofluid mechanics. *Annu. Rev. Fluid Mech.*, **18**, 91–147.
- Hua, B. L., and D. B. Haidvogel, 1986: Numerical simulations of the vertical structure of quasi-geostrophic turbulence. *J. Atmos. Sci.*, **43**, 2923–2936.
- Killworth, P. D., 1997: On the parameterization of eddy transfer. Part I: Theory. *J. Mar. Res.*, **55**, 1171–1197.
- Larichev, V. D., and I. M. Held, 1995: Eddy amplitudes and fluxes in a homogeneous model of fully developed baroclinic instability. *J. Phys. Oceanogr.*, **25**, 2285–2297.
- Lesieur, M., and J. Herring, 1985: Diffusion of a passive scalar in two-dimensional turbulence. *J. Fluid Mech.*, **161**, 77–95.
- Maltrud, M. E., and G. K. Vallis, 1991: Energy spectra and coherent structures in forced two-dimensional and beta-plane turbulence. *J. Fluid Mech.*, **228**, 321–342.
- Rhines, P. B., 1975: Waves and turbulence on a β -plane. *J. Fluid Mech.*, **69**, 417–443.
- , 1977: The dynamics of unsteady currents. *The Sea*, E. D. Goldberg et al., Eds., *Marine Modelling*, Vol. 6, Wiley and Sons, 189–318.
- Salmon, R., 1980: Baroclinic instability and geostrophic turbulence. *Geophys. Astrophys. Fluid Dyn.*, **10**, 25–52.
- Smith, K. S., and G. K. Vallis, 2001: The scales and equilibration of mid-ocean eddies: Freely evolving flow. *J. Phys. Oceanogr.*, **31**, 554–571.
- Spall, M. A., 2000: Generation of strong mesoscale eddies by weak ocean gyres. *J. Mar. Res.*, **58**, 97–116.
- Stammer, D., 1997: Global characteristics of ocean variability estimated from regional TOPEX/Poseidon altimeter measurements. *J. Phys. Oceanogr.*, **27**, 1743–1769.
- Stone, P. H., 1972: A simplified radiative-dynamical model for the static stability of rotating atmospheres. *J. Atmos. Sci.*, **29**, 405–418.
- Treguier, A. M., I. M. Held, and V. D. Larichev, 1997: On the parameterization of quasigeostrophic eddies in primitive equation ocean models. *J. Phys. Oceanogr.*, **27**, 567–580.
- Vallis, G. K., 1988: Numerical studies of eddy transport properties in eddy-resolving and parameterized models. *Quart. J. Roy. Meteor. Soc.*, **114**, 183–204.
- , and M. E. Maltrud, 1993: Generation of mean flows and jets on a beta plane and over topography. *J. Phys. Oceanogr.*, **23**, 1346–1362.
- Visbeck, M., J. Marshall, T. Haine, and M. Spall, 1997: Specification of eddy transfer coefficients in coarse-resolution ocean circulation models. *J. Phys. Oceanogr.*, **27**, 381–402.
- Wardle, R., and J. Marshall, 2000: Representation of eddies in primitive equation models by a PV flux. *J. Phys. Oceanogr.*, **30**, 2481–2503.
- White, A. A., and J. S. A. Green, 1984: Transfer coefficient eddy flux parameterizations in a simple model of the zonal average circulation. *Quart. J. Roy. Meteor. Soc.*, **110**, 1035–1052.
- Wunsch, C., 1997: The vertical partition of oceanic horizontal kinetic energy. *J. Phys. Oceanogr.*, **27**, 1770–1794.